



NorthWest Research Associates, Inc.

P.O. Box 3027 • Bellevue, WA 98009-3027

NWRA-CR-95-R135

3 April 1995

Annual Report
Covering the period February 18 1994 through 17 February 1995

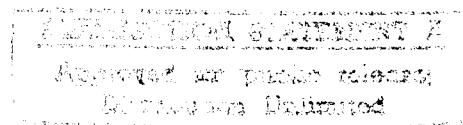
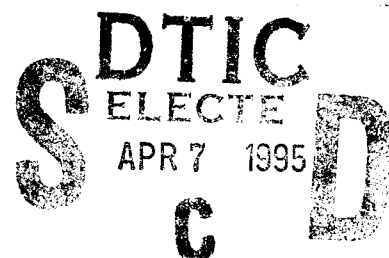
SEA ICE STRESS RESEARCH

Prepared by

Max D. Coon
Northwest Research Associates, Inc.
P.O. Box 3027
Bellevue, Wa. 98009

Prepared for
Dr. Thomas B. Curtin
Office of Naval Research
800 North Quincy Street
Arlington, VA 22217-5660

Contract No. N00014-92-C-0027



19950406 049

DTIC QUALITY INSPECTED 8

NWRA-CR-95-R135

3 April 1995

Annual Report
Covering the period February 18 1994 through 17 February 1995

SEA ICE STRESS RESEARCH

Prepared by

Max D. Coon
Northwest Research Associates, Inc.
P.O. Box 3027
Bellevue, Wa. 98009

Prepared for
Dr. Thomas B. Curtin
Office of Naval Research
800 North Quincy Street
Arlington, VA 22217-5660

Contract No. N00014-92-C-0027

Accession For	
NTIS	CRA&I <input checked="" type="checkbox"/>
DTIC	TAB <input type="checkbox"/>
Unannounced <input type="checkbox"/>	
Justification	
By <i>Per AID3178</i>	
Distribution /	
Availability Codes	
Dist	Avail and/or Special
<i>A-1</i>	

During last year, the Northwest Research Associates Arctic team completed the Spring SIMI field program in the Beaufort Sea. We have subsequently conducted data analysis and written papers on that data. In addition, we organized the Ice Mechanics and Arctic Modeling Workshop to be held in Anchorage, AK, April 25-28, 1995, which will report on the research findings of SIMI and will also address future research needs.

During this year, we presented a paper on Sea Ice Mechanics Initiative (SIMI) at the Offshore Technology Conference in Houston, TX, in May 1994. This paper was well received. The presentation was an attempt to foster communication between the Arctic research being done at the Office of Naval Research and the Arctic offshore-work of the oil industry. A copy of that paper entitled "The Sea Ice Mechanics Initiative (SIMI)," is attached. Also, the findings of our SIMI field work are reported in our paper entitled "Sea Ice Mechanics Research," which appears in Volume I of the Sea Ice Mechanics and Arctic Modeling Workshop proceedings. A copy of that paper is attached.

We have written a paper entitled "Forced-Displacement Measurements of a First-year Pressure Ridge and Keel" to be presented at Sea Ice Mechanics '95 Symposium as part of the ASME Joint Applied Mechanics and Materials summer meeting at UCLA in June 1995. A copy of this paper is attached. The results from this data analysis show that the strength of partially consolidated ridges changes in a period of two weeks from an active component in sea ice dynamics to an inactive component, because of its strength. We participated in the preparation of a second paper for the Ice Mechanics '95 Symposium with Dr. R. S. Pritchard of IceCasting and with Drs. D. M. Farmer and Y. Xie of Institute of Ocean Sciences. This paper, entitled "Acoustic Signatures of Falling Ice Blocks," examines the acoustic signature from small-scale processes associated with ridging, utilizing the data that we gathered with IceCasting and the Institute of Ocean Sciences during the Spring of 1994. A copy of this paper is attached.

Northwest Research Associates, Inc. organized the Sea Ice Mechanics and Arctic Modeling Workshop under the auspices of ONR, Mineral Management Services, and contributions from various oil companies as well as the Canadian National Energy Board. Volume I of the proceedings summarizes the Sea Ice Mechanics efforts by various P.I.'s in the SIMI program. A copy of the table of contents of Volume I is attached.

TABLE OF CONTENTS

Appendix A:	The Sea Ice Mechanics Initiative (SIMI)	A-1
Appendix B:	Sea Ice Mechanics Research	B-1
Appendix C:	Force-Displacement Measurements of A First-Year Pressure Ridge Keel	C-1
Appendix D:	Acoustic Signatures of Falling Ice Blocks	D-1
Appendix E:	Proceedings of the Sea Ice Mechanics and Arctic Modeling Workshop	E-1

THE SEA ICE
MECHANICS INITIATIVE
(SIMI)



OTC 7612

The Sea Ice Mechanics Initiative (SIMI)

M.D. Coon, G.S. Knoke, and D.C. Echert, Northwest Research Assocs. Inc.

Copyright 1994, Offshore Technology Conference

This paper was presented at the 26th Annual OTC in Houston, Texas, U.S.A., 2-5 May 1994.

This paper was selected for presentation by the OTC Program Committee following review of information contained in an abstract submitted by the author(s). Contents of the paper, as presented, have not been reviewed by the Offshore Technology Conference and are subject to correction by the author(s). The material, as presented, does not necessarily reflect any position of the Offshore Technology Conference or its officers. Permission to copy is restricted to an abstract of not more than 300 words. Illustrations may not be copied. The abstract should contain conspicuous acknowledgment of where and by whom the paper is presented.

ABSTRACT

The Sea Ice Mechanics Initiative (SIMI) is a five-year U. S. Navy Office of Naval Research (ONR) program. The main SIMI field experiment was in the Beaufort Sea from September 1993 through April 1994, with numerous other small field experiments, laboratory experiments, and modeling efforts. The goals of this program are to understand sea ice constitutive laws and fracture mechanics over the full range of geophysical scales, to determine the scaled responses to applied external forces, and to develop physically-based constitutive and fracture models. About twenty principal investigators are working to achieve these goals along with their associates. The SIMI experiments include ice stress, strain, strength, tilt, motion, temperature, and response to controlled load experiments. This work will provide new ice information for loads on structures and for Arctic operations, both private and government.

INTRODUCTION

The goals of the Sea Ice Mechanics Initiative (SIMI) Arctic research program are stated in the SIMI Summary Plan (Curtin, 1993). These are:

- Understand sea ice constitutive laws and fracture mechanics over the full range of geophysical scales and determine the scaled responses to applied external forces.

- Develop physically-based constitutive and fracture models.

These goals were developed at the Sea Ice Mechanics Workshop (Curtin, 1991), along with an assessment of the limits of current understanding, a list of priority research issues, and state-of-the-art methods for the many aspects of sea ice mechanics. Individual projects within the program were defined around the scale size used in the ice mechanics work.

This paper describes SIMI, focusing on the field program initiated in September 1993.

BACKGROUND

The Office of Naval Research held a Sea Ice Mechanics Workshop at Airlie, Virginia on November 12-14, 1990, where sea ice mechanics was examined from different perspectives, both methodological (theoretical modeling, laboratory experiments, and field observations) and behavioral (material, structural, and acoustical aspects). The Workshop Proceedings (Curtin, 1991) outline limits of current understanding, prioritizes research issues, and documents innovative methods of approach. The workshop participants included representatives from government agencies and laboratories as well as from universities, the oil industry, and other private sector engineers and scientists. The Workshop Proceedings were used to shape the five-year (1992-96) SIMI program.

ONR sponsored another workshop at Dunsmuir Lodge, Sidney, British Columbia, Canada on October 12-14, 1992 (Curtin, 1993). During this workshop, the detailed plan for SIMI was worked out. The main field experiment included a

Nomenclature and references at end of paper.

drifting camp in the Beaufort Sea collecting data from Fall 1993 through Spring 1994. The SIMI plan and the field program are described below in a quote from Curtin (1991).

"A major question in understanding and predicting the mechanical behavior of Arctic sea ice involves the effect of size on the dynamics. The notion that the scales of a specimen alone influences the operative physics has fundamental implications. The prime example is the pressure versus contact area relationship, suggesting a decrease in strength with an increase in size. There was consensus that obtaining a comprehensive quantitative relationship spanning from microscale to structural scale behavior is too ambitious on a five-year horizon; however, establishing the linkage between a few scales (e.g., centimeters to meters, meters to tens of meters) is achievable and should be pursued.

"Theoretical modeling is essential in relating behavior across scales and developing parameterizations. Improved models are required for both continuum and fracture behavior. Continuum and fracture models should be linked where possible. Small-scale laboratory experiments are required to link micromechanical properties with physical behavior and to identify mechanisms that may be important across scale. Intermediate scale laboratory tests under carefully controlled conditions can provide a crucial link between small and large scales. There was consensus on the need to establish the critical scales at which microscale processes become measurably important to larger scale behavior.

"Brittle or ductile sea ice behavior depends to a large extent on loading rates, which in nature typically range from 10^{-7} to 10^{-4} s^{-1} . Continuum behavior at different rates, particularly at larger scales, needs further investigation. Rate effects on fracture need to be quantified.

"While it is well known that temperature can determine elastic or viscous plastic behavior under isothermal conditions, the behavior of sea ice with realistic temperature gradients, as in the Arctic, remains to be characterized. The effects of temperature on fracture need to be resolved. Porosity, salinity, and microcrack distribution are important at small and medium scales. Gradients in these properties, in addition to those in thickness, degree of ridge consolidation, and macroflow distribution at larger scales, need to be ordered and quantified in the effects on the governing mechanics.

"Coherent and economical field tests designed to definitively relate forcing and response under the range and limits of conditions in nature are essential. Controlled loading tests in the field are necessary to understand large-scale behavior. In-situ ice properties and stresses can be monitored to some extent with current technology. Methods for more complete spatial mapping of these fields are needed. Techniques to measure three-dimensional flaw generation and distribution within full scale floes need development.

"The roles of mixed mode and non-simultaneous failure in reducing large-scale loads needs to be understood, as well as the important mechanisms in the initiation of long fractures (leads) in pack ice. The relative importance of bending, buckling, crushing, and crack nucleation/propagation in overall failure needs to be determined. Factors causing ice of the same thickness to ridge in some cases and raft (including finger rafting) in others need to be determined. Thermal stresses may be as important as mechanical stresses in preconditioning the ice for the propagation of cracks. The role of existing flaws and the residual stress state in the generation and propagation of long fractures requires study.

"The transition from laboratory to floe scales is best addressed within a hypothesis-testing framework. One hypothesis is that the behavior of samples under tensile stress and the distribution of this stress is most important in floe-scale cracking processes. Therefore, these stress conditions should be examined experimentally and parameterized in larger scale relationships that can be tested in floe experiments.

"Bridging the gap in understanding of ice processes from floe to regional scales may come from relating floe measurements to a viable statistical measure of the structure of regional scale distributions of ice. The measurements of environmental forcing and regional strain, for instance, can be related to average pack ice forces measured on the floe. Careful study of the relationships, particularly during deformation, should lead to improved regional constitutive laws. Also, fracture models developed for a single floe may be applicable to a collection of floes. Thus, selected geophysical parameters obtained from aerial or satellite imagery of a region combined with environmental forcing, will produce time-dependent theoretical and numerical models that can predict with improving degrees of skill the spatial distribution of new leads and ridges."

MODELING SUMMARY

The modeling studies included in the SIMI program are summarized below, grouped by scale size.

100 KM SCALE (PACK ICE)

- Coupled air-ice-ocean
- Fracture characteristics
- Deformation characteristics

10 KM SCALE (FLOE CLUSTER)

- Granular media rheology
- Anisotropic constitutive law

1 KM SCALE (FLOE, RIDGE, LEAD)

- Ridge building energetics
- Fracture mechanics, size effect

1-100 M SCALE (MACROCRACK)

- Thermal fracture
- Physically-based constitutive laws

- Fracture mechanics, size effects

1 CM - 1 M SCALE (MICROCRACK-CRYSTAL)

- Ductile-brittle transition, failure surfaces
- Crack nucleation

MEASUREMENT SUMMARY

The experimental studies in the SIMI program are summarized below, grouped by scale size.

100 KM SCALE (PACK ICE)

FORCING

Mechanical

- Regional surface winds (NOGAPS, NMC)
- Regional surface currents (GPS buoy array)

Thermodynamic

- Surface temperature (Argos buoy array)

DEFORMATION/FRACTURE

- Point strain field (Argos buoy array)
- Image strain field (satellite AVHRR, SSMI, SAR)

PROPERTIES

- Thickness distribution (low frequency acoustics)

10 KM SCALE (FLOE CLUSTER)

FORCING

Mechanical

- Stress on floes (GPS buoy array)

Thermodynamic

- Surface temperature (15 element GPS buoy array)

DEFORMATION/FRACTURE

- Image strain field (satellite SAR/ASF)
- Image strain field (satellite AVHRR, SSMI)
- Point strain field (15 element GPS buoy array)

PROPERTIES

- Thickness distribution (AUV)
- Ridge event distribution (SAR/ASF, AVHRR)
- Ice type distribution (SAR/ASF)

1 KM SCALE (FLOE, RIDGE, LEAD)

FORCING

Mechanical

- Wind, ocean stress (main floe station)
- Ice stress array (24-30 stress sensors)

Thermodynamic

- Surface temperature, radiation (main floe station)

DEFORMATION/FRACTURE

- Strain, tilt, acceleration (sensor clusters)
- Ridging event detection, localization (hydrophone array)

PROPERTIES

- Morphology, ridge-lead distribution (main floe survey)
- Thickness distribution (AUV, submarine)
- Ridge event distribution (SAR/ASF, AVHRR, buoys)

1-100 M SCALE (MACROCRACK)

FORCING

Mechanical

- Controlled loads (stress gauge array)

Thermodynamic

- Ice temperature profiles (thermistor arrays)

DEFORMATION/FRACTURE

- Event localization and magnitude (hydrophone, geophone arrays)
- Ridging event seismo-acoustic inversion (geophone, hydrophone arrays)
- Ridging deformation (high resolution GPS, stress sensors, tilt-strain meters, and inflatable air jack)
- Fracture energy, failure modes (first-year ice controlled load)
- Fracture energy distribution (first-year ice controlled load-acoustic, seismic response: borehole jack, hydrophone, geophone arrays)

PROPERTIES

- Seasonal evolution of elastic and shear wave properties and fissures on flat ice (controlled impulse source)
- Seasonal evolution of elastic and shear wave properties and fissures in ridged ice, crack event localization, failure mode detection (acoustic tomography)
- Seasonal evolution of ridge elastic, structural properties (coring, thermistor arrays)
- Seismo-acoustic scattering from ridges (pencil beam and explosive sources, hydrophone and geophone arrays)
- Block friction (in-situ tests)

1 CM - 1 M SCALE (CRYSTAL-MICROCRACK)

FORCING

Mechanical

- Experiments under controlled loads

Thermodynamic

- Surface temperature (NWS)

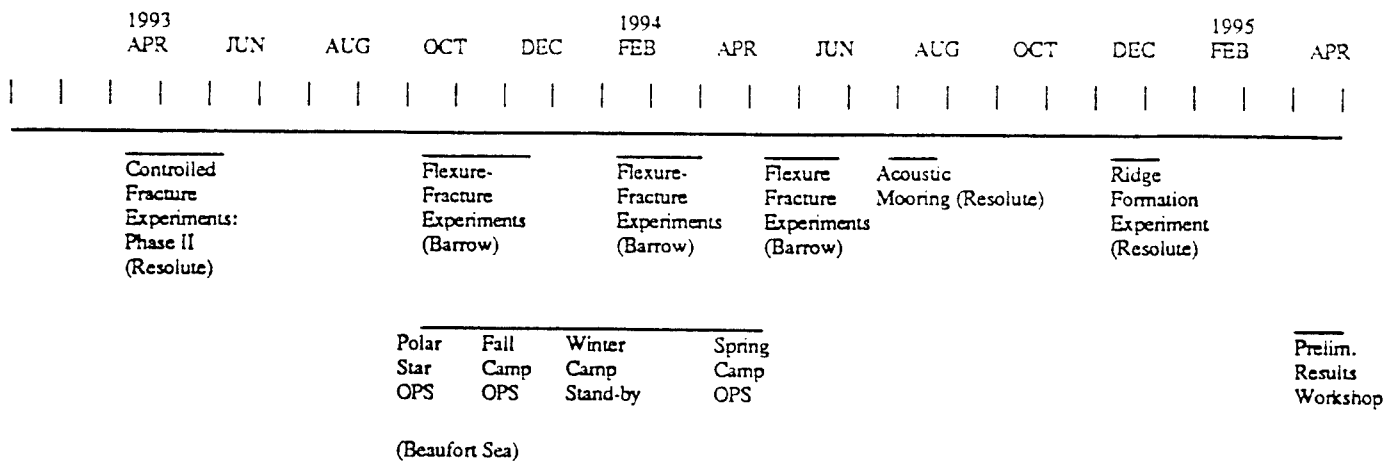
DEFORMATION/FRACTURE

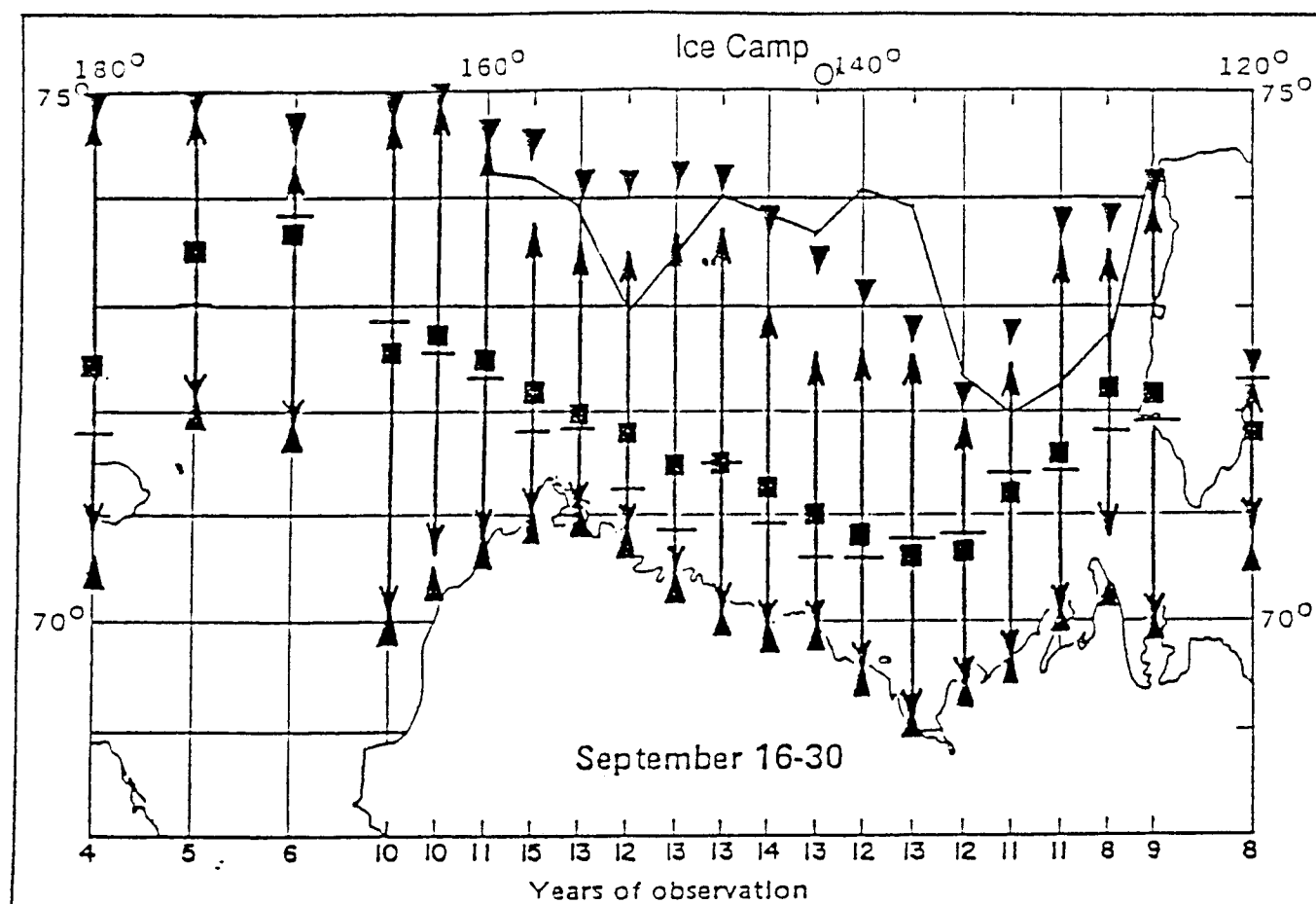
- Flexure, fracture related to microstructure (in-situ samples)
- Flexure, fracture related to microstructure (pit-pond tests)
- Fracture related to microstructure (testing machine)
- Low strain rate creep (testing machine)
- Internal friction, anelasticity (cyclic loading)
- Multiaxial compressive strength (pit-pond, testing machine)
- 3-D failure surfaces (testing machine)

PROPERTIES

- Microstructure linked with growth conditions (in-situ samples)

Figure 1 shows the SIMI experiment schedule, including tests near Resolute, Northwest Territories, Canada, near Barrow, Alaska, and in the Beaufort Sea. A workshop to present and discuss preliminary SIMI results will be scheduled in the first half of 1995.





Legend

- ▼ Extreme northern latitude
- ↑ Most northern latitude of 15-day means
- Median
- Mean
- ↓ Most southern latitude of 15-day means
- ▲ Extreme southern latitude

Source: G.J. Potocsky, 1975. *Alaskan Area 15- and 30-Day Ice Forecasting Guide*.

Figure 2. 1993 was an unusual ice year.

a week or two. This allowed the relatively small camp staff (five) to support over thirty science personnel. Most of the planned scientific experiments were accomplished or set up for winter-over data collection. The camp staff personnel left the camp on December 9, with the intent to return in the spring.

ICE FLOE CONDITION

The ice floe for the SIMI main camp was like an uneven grillage in the sense that it had multi-year ice perforated with many holes formed by melt ponds. It was similar to six other floes that were drilled except for the runway, in which much of the ice was 90 cm thick. The runway had thick multi-year ice on three sides of it; however, there were places where the runway ice was only 30 cm thick. The 90-cm ice was apparently formed by a triple raft. On further examination, it was determined that this "floe" was formed from two pieces of multi-year ice which came together and formed the runway by rafting. The west end of the floe (about 1/3) was not truly part of the "floe" but was separated pieces of multi-year ice embedded in thin (30 cm) ice which also connected them to the floe. The floe boundary was defined by a "line" of pressured ice (blocks pushed up) but not ridged ice.

One of the reasons for a fall SIMI program was to see how a multi-year floe changed through the fall, winter, and spring. To this end, this year was good for the experiment.

Some observations of note. There were many 'ridged' areas that were not winter ridges of first-year ice with typical sail and keel. These ridges were formed from single (maybe a few) blocks of old ice pushed up to form a ridge with a sail but no keel. This floe was considered to be 'near the ice edge' even though it was at 75°N because it was in such an extreme condition of melt.

ICE DRIFT

The ice drift of the main camp is shown in Figure 3 through January 1994. With some data gaps, the '+' marks represent the main camp GPS buoy position every six hours. Each part of the figure shows the whole trajectory through the end of the month indicated. The cluster of points encircling both ends of each trajectory indicate the positions of fourteen GPS buoys deployed by PMEL around the main camp. Although there are some data gaps, the relative motion of the surrounding buoys are small, less than 3 km. These data will be combined with ice stress data as described in Coon et al. (1993) to analyze the energy dissipation in the pack ice surrounding the main camp for the development of a pack ice anisotropic constitutive law (Coon et al, 1992).

DISCUSSION AND FUTURE PLANS

Since the plan was to reoccupy the fall experiment site in the spring, we had to take into account the expected drift of the ice when choosing the location in the fall. Since the fall effort was supported and recovered by airplane, the site needed

to be within Twin Otter range from shore. For this reason, the fall experiment site was chosen to be 500 km northeast of Deadhorse. Because of the light ice year, however, the camp was established further north and west than planned to remain 500 km from Deadhorse.

The floe for the camp had a location for an ice runway; it was not possible, however, to land a Twin Otter on September 29 when the Polar Star was to leave. Therefore, a crew of four was left at the ice camp with plans to resume full operations in late October 1993 when the runway ice was colder and stronger. SIMI has demonstrated that it is possible to establish an ice camp (which can be later supported by aircraft) in the fall from an icebreaker, even in a light ice year.

As of this writing, the ice camp has drifted to 74°40'N, 155°W, roughly north of Barrow, Alaska. Should the camp remain within 500 km of a useful airfield, the spring field operations will continue as planned. If, however, the camp drifts too far out or the main floe is unusable, the scientific and ice camp equipment will be recovered in a prudent manner and a new ice camp will be established north of Deadhorse, Alaska, for the spring field operations.

ACKNOWLEDGMENTS

We wish to acknowledge Dr. Tom Curtin of ONR for sponsoring the SIMI program. We wish to thank Capt. R. J. Parsons ("Never say 'no' to the Science Team") and the eager and highly professional crew of the U.S.C.G.C. Polar Star, as well as Mr. Andreas Heiberg and the dedicated logistics team from the University of Washington's Polar Science Center. Finally, we wish to thank Dr. Jim Overland and Ms. Sigrid Salo of PMEL for Figure 3. The author's work was funded by ONR contract number N00014-92-C-0027.

NOMENCLATURE

ASF	Alaska SAR Facility
AUV	Autonomous Underwater Vehicle
AVHRR	Advanced Very High Resolution Radiometer
GPS	Global Positioning System
NMC	National Meteorological Center
NOGAPS	Navy surface wind analysis code
NWS	National Weather Service
ONR	Office of Naval Research
SAR	Synthetic Aperture Radar
SIMI	Sea Ice Mechanics Initiative
SLAR	Side Looking Airborne Radar
SSMI	Special Sensor Microwave Imager
PMEL	National Oceanic and Atmospheric Administration's Pacific Marine Environmental Laboratory
USCG	United States Coast Guard

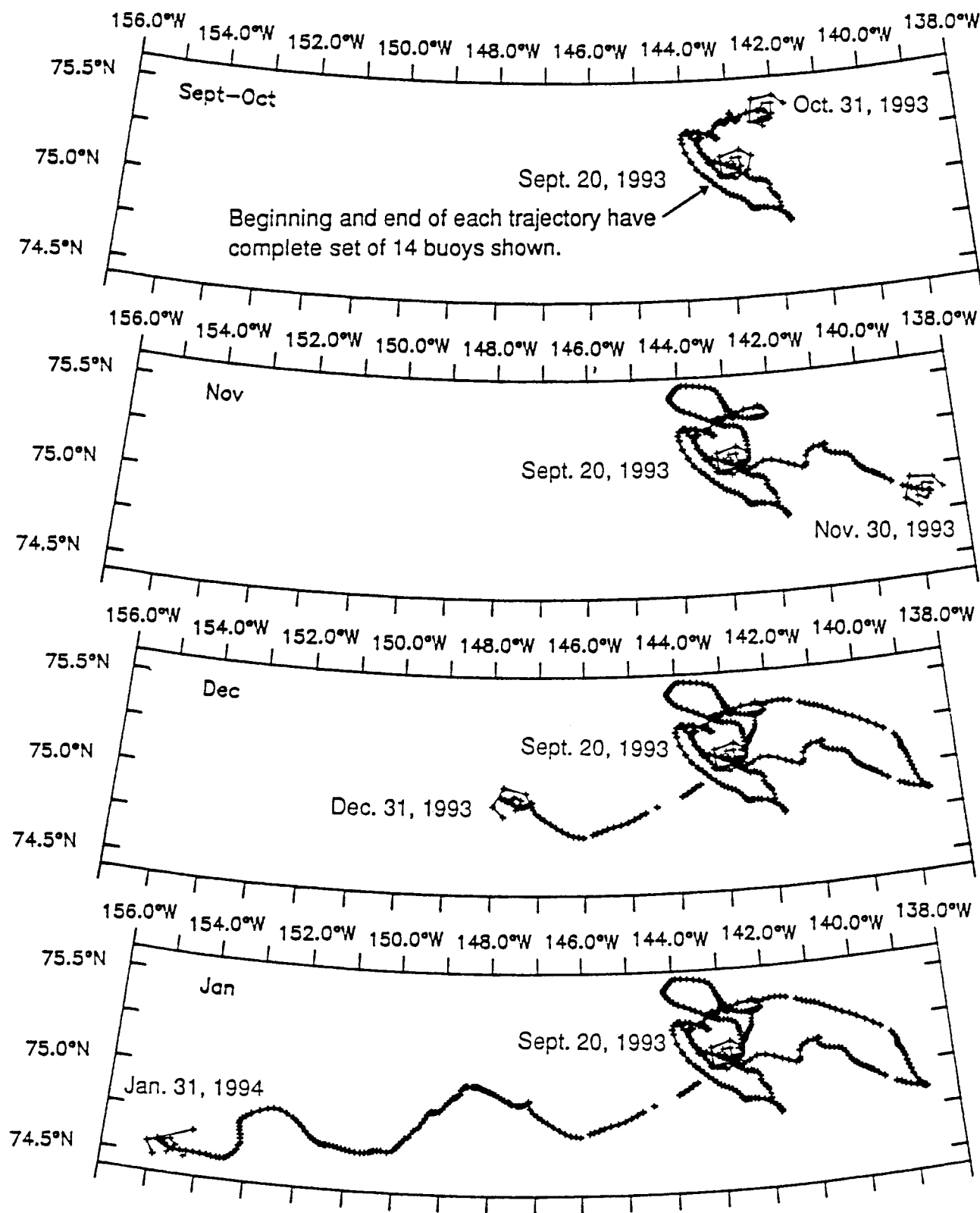


Figure 3. SIMI Ice Camp Drift (with six-hour data intervals)

REFERENCES

- Brower, W. A., Jr., H. F. Diaz, A. S. Prechtel, H. W. Searby, and J. L. Wise (1977) Climate Atlas of the Outer Continental Shelf Waters and Coastal Regions of Alaska, Vol. III, Chukchi-Beaufort Sea, U. S. Department of Commerce, National Oceanic and Atmospheric Administration, Alaska Outer Continental Shelf Environmental Assessment Program (OCSEAP) Final Report -- Research Unit 347.
- Coon, M. D., G. S. Knoke, and D. C. Echert (1992) "Pack Ice Anisotropic Constitutive Model," IAHR 92, Proceedings of the 11th International Symposium on Ice, Banff, Alberta, June.
- Coon, M. D., G. S. Knoke, D. C. Echert, and H. L. Stern (1993) "Analysis of Contemporaneous Measurements of Pack Ice Stress and Ice Strain Measurements from SAR Imagery," OCEANS'93, Victoria, B.C., Canada, October.
- Curtin, T. B. (Editor) (1991) "Air-Ice-Ocean Interaction: Lead Dynamics, Ice Mechanics, Ice Acoustics; Proceedings of the Sea Ice Mechanics Workshop, 12-14 November 1990, Airlie, Virginia," Office of Naval Research, Arlington, VA, April.
- Curtin, T. B. (Editor) (1993) "Sea Ice Mechanics Initiative (SIMI), Summary Plan, FY94-95," Office of Naval Research, Arlington, VA, August 27.

SEA ICE
MECHANICS RESEARCH

Sea Ice Mechanics Research

Dr. Max Coon (P.I.), Mr. Skip Echert, and Dr. Stu Knoke of Northwest Research Associates (NWRA).

Scope of Model and/or Data Set

The NWRA team performed a variety of experiments during the SIMI field program: ice-stress measurements, controlled-load and noise-generation tests, ice-on-ice friction tests, ridge-strength tests, and a multiyear floe evolution study.

Ice-Stress Measurements -- NWRA successfully deployed flatjack, fluid-filled stress sensors with an automatic pressurization-check feature in an autonomous station configuration. We installed these sea-ice-stress "buoys" at four sites; each buoy measured ice stress in four directions, from which we will derive the ice-stress state in the horizontal plane. A ridging event buried the first buoy, installed near Mt. Curtin at the West SIMI Ice Camp (Map 2, E7), after one month. The second buoy, installed about two miles north of West Camp on Floe 4 (Map 1, E4), operated continuously for over nine months. The crack that flooded portions of the West Camp disabled the third buoy after three months (Map 2, F5), but we repaired it and operated it for an additional three weeks at the East Camp (Map 4, C6). Table 1 lists the operational lifetime of the four buoy installations and the number of thermistors used to measure ice temperatures. The buoys wrote ice stress to an internal storage module at five-minute intervals and transmitted ten-minute data through the Argos satellite relay system. The buoys also stored and transmitted temperature readings from the higher (colder) two thermistors on the same schedule but stored and transmitted the lower (warmer) thermistor readings and a battery voltage every six hours.

Table 1. Ice-stress buoys

Buoy number	Test site	Start date	End date	Number of thermistors
1	Mt. Curtin	29 Oct. 93	4 Dec. 93	4
2	Floe 4	31 Oct. 93	3 Aug. 94	4
3	Lake Andy	22 Nov. 93	25 Feb. 94	8
4	East camp runway	1 Apr. 94	23 Apr. 94	8

In support of the sea-ice-stress buoys, NWRA performed various other ice-stress sensor experiments at 22 locations near the two ice camps:

- Individual stress sensor measurements,
- "High-data-rate" stress tests with data collection rates to 4 Hz,
- "Sensor/ice contact" tests to check contact between the sensor and the ice,

- "Inclusion" tests to calibrate the response of the stress gauge to the ice stress produced by an air jack a few decimeters away, and
- Comparison tests with other types of ice-stress and strain sensors.

We installed and tested individual stress gauges at the 22 locations listed in Table 2. Dataloggers generally collected this stress and temperature data at five-minute intervals. The two winter-over sites also collected temperature data hourly. The first site (Map 2, F4) tested the installation of a stress gauge in the low, flat, multiyear hummocks in the early autumn. The second site (Map 2, F5) tested the freeze-in of gauges installed at various depths in autumn first-year ice; the lowest was half in the water at installation. The sensors at the third site (Map 2, F5) were installed identically to the stress sensors on the buoys to obtain inclusion test data to support the interpretation of the buoy data. The fourth site (Map 2, F4) again tested the installation of stress gauges in the low flat hummocks of multiyear ice in the autumn. The fifth site (Map 2, E3) was used for the comparison tests in the West camp runway ice. The sixth site (Map 2, E5 and F5) studied the horizontal and vertical variation of ice stress in a large area of flat first-year ice, Lake Andy. (We hypothesize that Lake Andy had been a large, bottomless melt pond during the previous summer.) The seventh site (Map 2, F4) studied the local variations of ice stress near a hummock. The final site (Map 4, C6) was installed for inclusion test data to support the nearby stress buoy.

Table 2. Individual ice-stress gauge sites

Site number	Test site	Start date	End date	Number of stress gauges	Number of thermistors
1	Study area	23 Sept. 93	27 Sept. 93	1	0
2	Lake Andy	27 Sept. 93	16 Nov. 94	5	0
3	Lake Andy	15 Nov. 93	28 Nov. 94	3	2
4	Study area	17 Nov. 93	21 Nov. 93	2	2
5	West camp runway	18 Nov. 93	26 Nov. 93	2	2
6	Lake Andy	29 Nov. 93	27 Feb. 94	4	2
7	Study area	30 Nov. 93	17 Mar. 94	3	2
8	East camp runway	5 Apr. 94	23 Apr. 94	2	0

"High-data-rate" is a relative term; we use it to mean data rates of one to four readings per second as compared to our standard interval of five minutes. We performed high-data-rate tests with one to four stress sensors at a time, looking for stress signals we otherwise would have missed due to sampling rate. We also obtained ice-stress data at one-second intervals for six 15-hour periods and at 1/4-second intervals for one three-hour period.

Two methods were used to evaluate stress sensor installations: sensor/ice contact tests and inclusion tests. Turning a screw-plunger assembly added additional fluid to each ice-stress sensor to assure good contact with the surrounding ice. The additional fluid caused

either an abrupt increase in fluid pressure in the sensor or no response at all. The stress buoys performed these tests automatically on a schedule, which proved useful for timing the melt-out in the spring. Each stress sensor received one or more sensor/ice contact tests; the response varied with season, ice temperature, and ice type. If the sensor showed an increase of at least 50 kPa during the test, we considered the sensor to be in good contact with the ice. Sensors that failed the test also failed to respond to air jack stress and natural ice stress.

Air jacks were used to perform inclusion tests, which were stress sensor response tests at geophysical stress levels (0 to 300 kPa) and geophysical loading rates (1 to 100 kPa/min.). We used a square, flat, air jack about 0.6 meter on a side to apply pressure to ice containing one or two sensors. We performed "square-wave" tests, for which we adjusted the air jack pressure in an on-off cycle, and "ramp" tests, for which we adjusted the pressure in a slow-increase, slow-decrease pattern. The square-wave test was a quick gauge calibration, but the ramp test simulated realistic loading rates based on our prior field data. We measured the stress-sensor inclusion factor on 20 sensor installations. Both 15-cm and 20-cm diameter sensors were tested using square-wave and ramp tests. On the square-wave tests, the air jack pressure was varied from 20 kPa to 200 kPa above ambient; on the ramp tests, the air jack pressure was 100 to 200 kPa above ambient. The square-wave tests typically had a cycle period of a minute, while each up and down ramp test took from one to three hours.

In cooperation with Jackie Richter-Menge from the Cold Regions Research and Engineering Laboratory (CRREL) and Dr. Peter Wadhams from the Scott Polar Institute (SPI), we performed a test series to provide a head-to-head comparison of the CRREL three-wire stress sensor with the NWRA flatjack sensor and of the SPI strain gauge with the NWRA flatjack sensor. We ran a set of square-wave tests and a ramp test. In each, the air jack pressure was varied from ambient to about 60 kPa above ambient, and the resulting stress and strain sensor readings were recorded.

Controlled-Load and Noise-Generation Tests -- NWRA, working with Dr. Robert Pritchard of IceCasting, Inc. (ICI), performed over 30 controlled-load tow tests and 40 other tests to generate various types of the noise representing potential Arctic acoustic sources. These tests were performed at the Football Field (Map 4, D6), East Pond (Map 4, C6), South Camp (about 18 km south of East Camp), and the IOS site (Map 4, B6). Dr. Henrik Schmidt's group from MIT/WHOI and/or Dr. David Farmer's group from the Institute for Ocean Sciences recorded the acoustic signals generated by many of these tests with hydrophones and/or geophones. The tow tests consisted of towing a block of ice on partially submerged ice to simulate rafting, on snow-covered or bare ice to simulate over-ride, and under young ice to simulate under-ride. On each of the tow tests, the tow load was usually recorded at 16 Hz and showed irregular slip-stick oscillations. We also measured the tow speed, the block dimensions and weight, and the snow thickness so that we could calculate the minimum and maximum sliding friction coefficient.

The other tests included dropping blocks onto ice, flopping blocks onto snow-covered or bare ice, tipping blocks into water, tipping blocks underwater to float up, releasing blocks underwater to bounce on the bottom of the ice, and breaking cantilever beams. Table 3 lists these acoustic experiments.

Table 3. Acoustic Source Tests

Block Motion	Number of Tests	Number of Unique Blocks Used for Test Series
Flop onto bare ice	5	5
Flop onto snow	7	5
Drop	10	9
Splash	2	2
Underwater flop	2	2
Underwater bounce	7	2
Cantilever beam	3	3

Ice-on-Ice Friction Tests -- During April 1993, NWRA ran a series of tests to measure the ice-on-ice friction coefficients on "natural" cracks generated in the sea ice near Resolute, NWT. These tests were conducted in conjunction with Dr. John Dempsey of Clarkson University, who conducted sea-ice fracture and ice characterization tests. All of these tests were performed in the 1.8-meter thick, first-year sea ice in Allen Bay. The test parameters are listed in Table 4.

Table 4. Test Parameters for Ice-on-Ice Friction Tests

Normal air pressure (kPa)	Number of tests	Total face displacement (mm)
40	7	13-65
200	8	41-54
400	4	38-93
Varied 15-170	2	77-89

Ridge-Strength Tests -- NWRA ran strength tests on first-year ridged ice using the air jack to simultaneously load the ice and measure the displacement. In November, we obtained underwater video and one inflation sequence of the air jack in the keel at the bog site (Map 2, H5). In April, we characterized the sail and keel geometry of a ridge formed from first-year ice, inflated the air jack in four slots, and recorded the acoustic emissions during the air-jack tests at our ridge site (Map 4, A4). The ridge configuration in the vicinity of the four air-jack slots was characterized by drilling 12 holes and through observations with an underwater camera (but no video tape). Dr. Robert Pritchard recorded the noise using Dr. David Farmer's hydrophone equipment.

Multiyear Floe Evolution Study -- We studied the evolution of a 60-by-60-meter area of multiyear ice near the SIMI West Camp by measuring ice thickness, snow cover, ice temperature, ice salinity, and ice stress (Map 2, F4). Our dataloggers recorded ice temperatures at three depths at four sites every hour from September 1993 to March 1994. We measured ice salinities from core samples taken in September. We also made aligned ice-stress measurements at three sites from November 1993 to March 1994. Ice thickness and snow cover were measured in September and March at nine locations in the study area. We obtained underwater video of the bottom of the ice in September through four holes in the ice using an underwater camera mounted on a pole. Also, U.S. Coast Guard divers from the USCGC Polar Star took underwater videos of the underside of the ice in September with a hand-held camera.

Findings to Date

Ice-stress Measurements -- NWRA buoys measured comparable ice-stress events lasting three to nine days in December (days 350-358), February (days 33-35), and April (days 91-95), as can be seen in Figure 1. Figure 1 shows six-hour samples of the stress-sensor oil-pressure data transmitted via Argos satellite for the full life of the buoy, including spikes resulting from the auto-pressurization cycles. There were no major stress events after mid-May, and the ice apparently melted away from the sensors in early July, totally relieving all residual ice stress around the sensors.

We found comparable stress in the first-year ice on opposite sides of a hummock but much lower stresses in the hummock itself. Some hummocks were strong ice (the stress gauges responded as though they were in lake ice), but others were very soft or porous ice since the stress gauges did not respond to sensor/ice contact tests or inclusion tests. We also found significant stress variations across the length of Lake Andy, a large area of first-year ice surrounded by multiyear ice. We hypothesize that a slip-stick ice motion event caused the most interesting signal which we recorded during the high-data-rate tests (Figure 2). From the inclusion tests, we found that, at these load values and load rates, the sensor response is significantly lower than prior laboratory measurements indicate, implying that ice-stress levels may be two to five times more than the measured sensor fluid pressure.

Controlled-load and Noise-generation Tests -- Blocks of ice sliding over or under flat ice generally exhibited slip-stick behavior with large fluctuations in the sliding friction, as illustrated for the tow load history in Figure 3. Figure 3 shows the first 12 seconds of Test 8-13, a dry over-ride test; the signal almost immediately settles into a repetitive slip-stick pattern. The load fluctuations on the ramp-ups are caused by cable oscillations since the ice block was stationary during those times. The ice-deformation mechanisms that generated more acoustic noise were blocks dropping or flopping onto bare ice, blocks sliding over snow-covered ice, and blocks falling into the water. Quiet ice-deformation mechanisms included blocks sliding or bumping underwater, rafting (lubricated by water), and blocks dropping or flopping onto snow-covered ice.

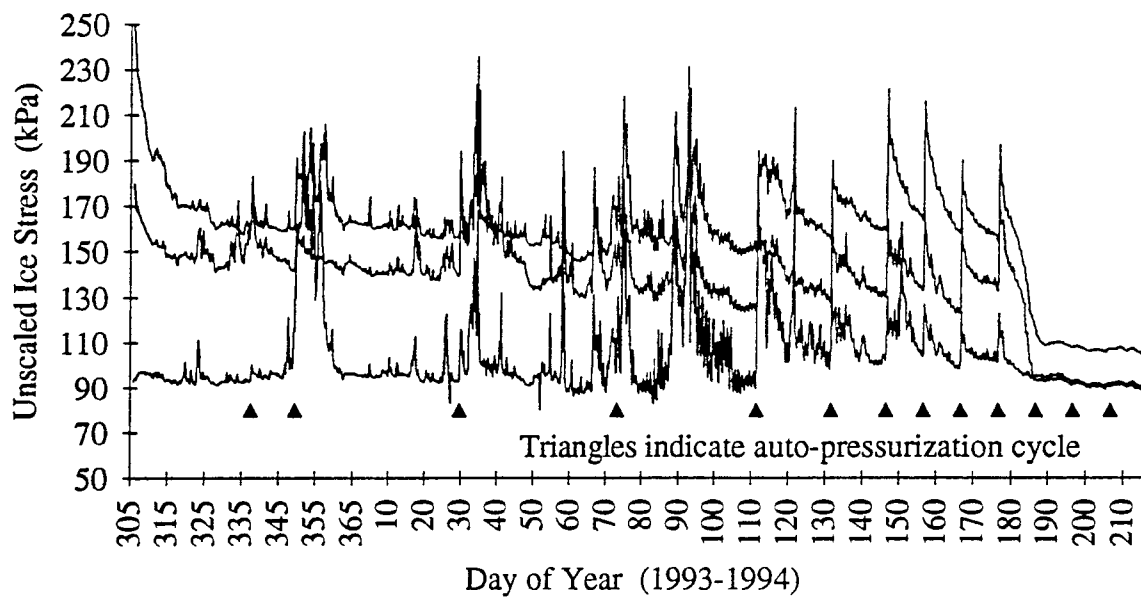


Figure 1. Ice-stress Buoy 2 (Floe 4) data via Argos, Nov. 1, 93 - Aug. 3, 94

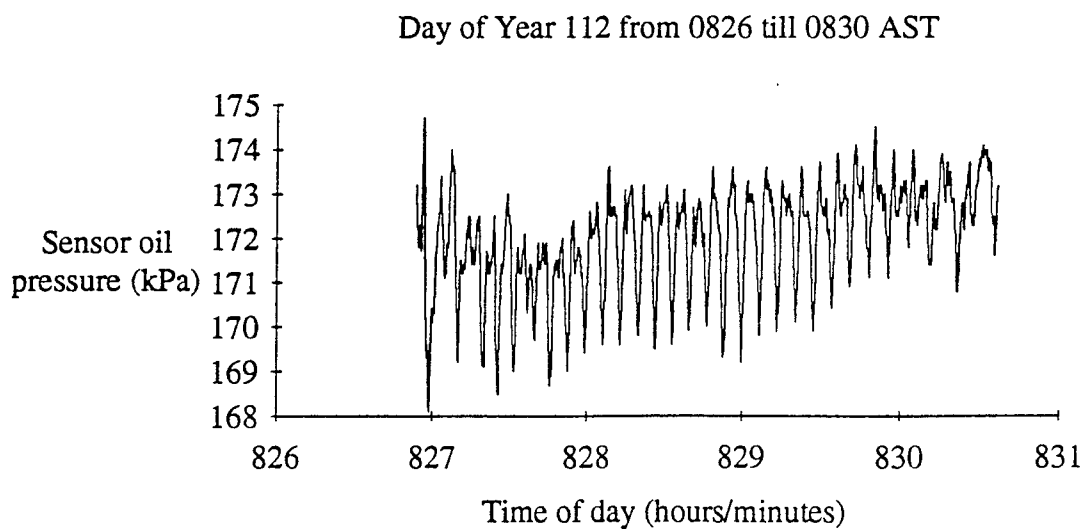


Figure 2. Ice-stress signal recorded near East Camp

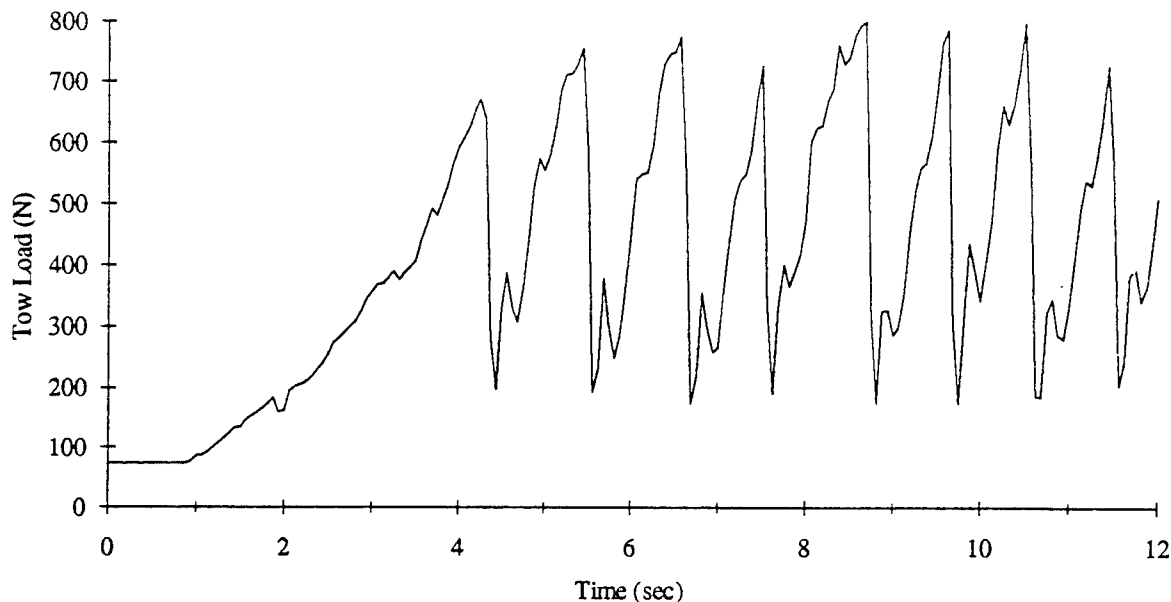


Figure 3. Tow load time series from an over-ride test (Test 8-13)

Ice-on-Ice Friction Tests -- In the configuration tested at Resolute, the shear force to cause shear motion along a fresh crack was surprisingly steady and smooth, except for the initial start-up motion. This may have resulted from having an air jack provide the normal force and a hydraulic jack provide the shear force. These dynamics are very different from an ice block being pulled with a winch. The measured coefficients of friction of natural cracks in first-year sea ice are consistent with the friction angle of pack ice calculated from ice-stress measurements made during the CEAREX program.

Ridge-strength Tests -- The strength of the fused ice in the ridge was highly variable, ranging from essentially solid ice near the surface to loose pieces floating underwater at or near their melting point temperature. Figure 4 shows an intermediate case of air jack pressure versus time. We interpret the down steps during the long rise as ice-to-ice contacts breaking and slipping. We stopped the displacement of the air jack when it had reached maximum stroke. We caused the large down step at the end by releasing the pressure in the air jack. These tests suggested that a better test of ridge keel strength would require a larger volume displacement, on the order of 8 cubic meters or more.

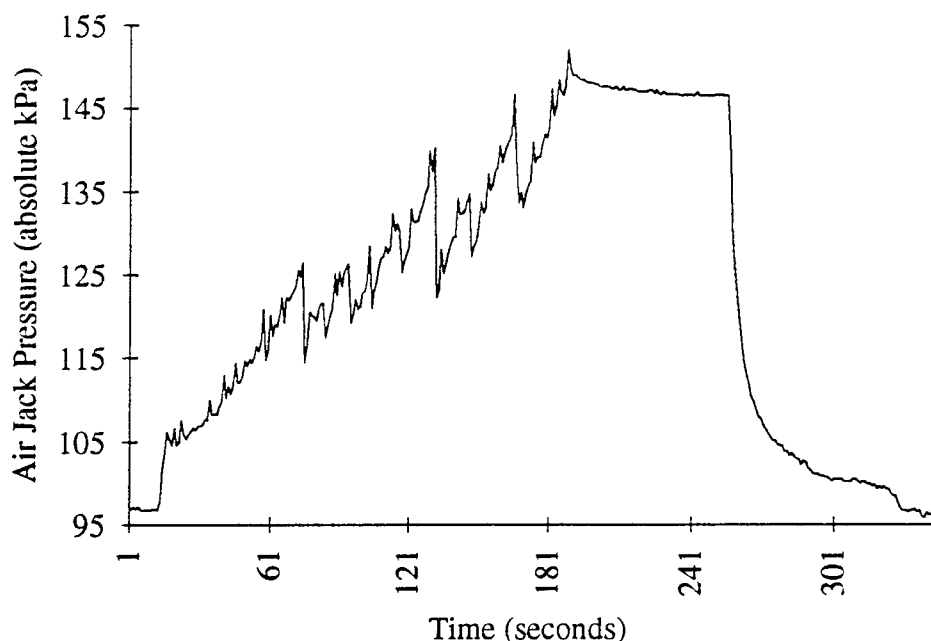


Figure 4. Air jack pressure versus time for one ridge test (results were highly variable).

Multiyear Floe Evolution Study -- In September, the study area consisted of hummocks and melt ponds covered with 20 cm of saline first-year ice. The multiyear ice had a highly porous bottom layer with a rough, lumpy appearance. The five separate melt ponds in the study area were small (two to ten meters across) and the surrounding hummocks protected their first-year ice from ice deformations. Some of the melt ponds had about 40 cm of salt water beneath the first-year ice and about 50 cm of multiyear ice beneath the water; others had nothing but water beneath the first-year ice. Before the first snowfall, the area looked like a huge slice of Swiss Cheese; melt ponds were the holes. The underside of the study area ice also had a unique appearance, with large flat areas of first-year ice separated by lumpy, steep-walled keels. By spring, the melt pond ice was about 1.2 meters thick with 0.5 to 1.5 meters of snow cover, but two- to four-meter keels still separated the flat ice segments. The multiyear ice underlying the salty melt ponds had also grown, about 10 cm.

Analysis and Publication Plans

Our first priority has been to document our SIMI test results in the above categories. We plan to analyze all field data collected during SIMI, including the data from the ice friction experiments conducted at Resolute earlier in 1993. We plan to publish papers and make presentations at the AGU, Oceans, ISOPE, and OTC Conferences. The following is a list of titles for potential papers and/or presentations resulting from our SIMI work:

- Interpretation of inclusion factor tests on flat-jack ice-stress sensors
- Estimates of first-year ridge strength from field measurements
- Acoustic emission of simple motions of sea-ice blocks
- In-situ measurements of ice-on-ice sliding friction
- Analysis of long-term sea-ice-stress measurements
- Validation of an oriented pack ice constitutive law with SAR, GPS, and sea-ice-stress measurements
- Performance comparison of two ice-stress sensors and an ice strain sensor
- Jay's Fingers -- a documented example of the rafting of very thick sea ice
- Chaotic dynamics of the slip-stick behavior of moving blocks of sea ice

Following is a list of our recent publications resulting from the SIMI program and relevant publications on models and equipment used during the SIMI program:

- "The Sea Ice Mechanics Initiative (SIMI)," M. D. Coon, G. S. Knoke, and D. C. Echert, in *Proceedings of the 1994 Offshore Technology Conference*, Houston, TX, May 2-5, 1994.
- "Contemporaneous Field Measurements of Pack Ice Stress and Ice Strain Measurements from SAR Imagery," M. D. Coon, G. S. Knoke, D. C. Echert, and H. L. Stern, in *Proceedings of OCEANS 93 Conference*, Victoria, B.C. Canada, October 18-21.
- "Phenomenological Constitutive Model for Columnar Ice," M. D. Coon and G. S. Knoke, in *ISOPE-93 Singapore: The 3rd International Offshore and Polar Engineering Conference*, Singapore, June, 1993.
- "Pack Ice Anisotropic Constitutive Model," M. D. Coon, D. C. Echert, and G. S. Knoke, in *IAHR 92, Proceedings of the 11th International Ice Symposium*, Banff, Alberta, June 15-19, 1992.
- "Arctic Ice Stress Measurements," P. A. Lau and G. S. Knoke, in *Proceedings of OCEANS'91 Conference*, Honolulu, October, 1991."

*FORCE-DISPLACEMENT MEASUREMENTS OF
A FIRST-YEAR PRESSURE RIDGE KEEL*

FORCE-DISPLACEMENT MEASUREMENTS OF A FIRST-YEAR PRESSURE RIDGE KEEL

**Max D. Coon
Douglas C. Echert
Gerald S. Knoke**

Northwest Research Associates, Inc.
Bellevue, Washington

ABSTRACT

The strengths of the consolidated and partially consolidated parts of a first-year sea ice ridge keel may be the design parameters for structures to be placed in regions covered seasonally by first-year ice. These strengths are also important for large-scale ice dynamics models which can account for leads and discontinuous ice motion. The strength of a first-year, partially consolidated keel has not been measured with certainty because of the heterogeneous nature of the broken ice and the large size of the keel. The authors have developed and have performed an initial field test of a system to measure the strength of a first-year partially consolidated keel. The system consists of a wheeled chain saw, a 60x60x2-cm air jack (a stiffened rubber bladder), an air compressor, and an air pressure recorder. After removing a portion of the sail of the test ridge, the wheeled chain saw is used to cut a vertical slot into the keel for the air jack. Inflating the jack provides the pressure-displacement curve which in turn provides the limit load of plastic deformations of the keel, an index of keel strength. Four measurements were made on a small, first-year ridge in the Beaufort Sea during April of 1994. The maximum pressures were variable: 20, 40, 210 and greater than 700 kPa. Calculations of the load for a continuing motion solution based on laboratory test data on unconsolidated rubble resulted in a significantly smaller value than the measured limit load. We believe significant consolidation of the keel occurred in the two weeks between the ridging event and our tests. The fully consolidated layer between the sail and keel generally provides the majority of the ridge strength. Future work should include tests of a ridge in fall, winter, and spring to track strength with consolidation.

INTRODUCTION

First-year ridges can control the total load on structures in parts of the Arctic (Wang and Poplin, 1995). First-year ridges are also involved in the dynamics of pack ice through the ice thickness distribution (Thorndike et al., 1975) and, in models such as the oriented pack ice constitutive law, the large-

scale strength (Coon et al., 1992). The strength of ridges is as important as the ridge shape, frequency of occurrence, and keel depth because the strength is required to determine the load on a structure or ship as well as the amount of force that pack ice can transmit. Field measurements of ridge strength provide scale for laboratory measurements done on the friction and cohesion of broken ice in a shear box (Ettema and Schaefer, 1986; Ettema and Urroz, 1989; Keinonen and Nyman, 1978; Urroz and Ettema, 1987; Weiss et al., 1981; and Wong et al., 1987). For example, Prodanovic (1979) ran laboratory model tests to measure the shear strength and the simulated loads on cylindrical structures. Allyn and Wasilewski (1979) analyzed the strength of rubble fields in connection with artificial islands. The laboratory tests, however, are nearly always performed on unconsolidated ice blocks. As a ridge gradually changes from being unconsolidated through partially consolidated (as ours was) to a fully consolidated multi-year ridge, its strength increases.

This paper presents a description of the ridge tested (block size distribution, porosity, temperature, and salinity) followed by the test procedure, the test results, hindcast analysis, and discussion.

EXPERIMENT

The force-displacement measurements of a first-year pressure ridge keel were made about 500 km north of Prudhoe Bay, Alaska on April 14-16, 1994, with multi-year ice on both sides of the ridge and refrozen lead studied. The equipment for this experiment was tested in the fall of 1993, and data were collected in the spring of 1994 with modified equipment (see Coon et al., 1994). The strength of first-year ridged ice was measured using an air jack (a stiffened rubber bladder) to simultaneously load the ice and measure the displacement. In addition, we characterized the sail and keel geometry of a ridge formed from first-year ice, and inflated the air jack in four slots. The ridge configuration in the vicinity of the four air-jack slots was characterized by drilling 12 holes and with observations with an underwater camera.

The ridge was selected by searching the area around the SIMI East Camp from a helicopter, looking for a crisp, new, first-year ridge. The ridge was about 2 km from the SIMI camp, which was manned during the formation of the lead from which the ridge was built and during the ridge building.

Ridge data

Holes were drilled to establish the extent of the keel and refrozen lead ice. The lead ice had ridged against a multi-year floe, causing a large block of multi-year ice to fracture and tilt down. The refrozen lead ice had continued to grow thicker after the ridging event, which probably took place on March 30. After looking at the underside of the test area with an underwater video camera using poles inserted through other holes in the ice for visual reference, we cleared off some sail blocks and selected the locations for cutting slots for the air jack.

Block size distribution. Nearly all the blocks in a 100 block survey of the ridge sail had a thickness of 0.14 m. Their longest dimension averaged 0.49 m with a standard deviation of 0.29 m. Based on their average width, the block area averaged 0.20 m² with a standard deviation of 0.22 m². These results are typical for ridges built from first-year ice, falling between the two empirical fits provided in Tucker and Govoni (1981) on their Figure 10.

Porosity. To establish the location of voids in the keel near the air jack slots, three sets of holes were drilled and logged. Figure 1 shows the plan view of the slots and the holes; there are two rows of holes outside the test area and a set of holes drilled alongside the slots after the force-deformation tests. Figure 2 illustrates the locations of the voids in the two rows of holes. The sail is to the left in

these figures while the 0.46 m refrozen lead ice is to the right. Each hole drilled started with a hard, solid layer which averaged 0.56 m thick; at the bottom of that layer, we hit softer ice or a void. After the force-deformation tests, the holes shown in Figure 3 were drilled and logged. Hole numbers 12 and 13 were drilled alongside the slots for Tests 1 and 2; holes 14 and 15 alongside Test 3; and holes 16 and 17 alongside Test 4. The average porosity for all the holes was 25 to 35%, depending upon whether mushy soft ice is considered as solid ice or void. These results are similar to those of Frederking and Wright (1982).

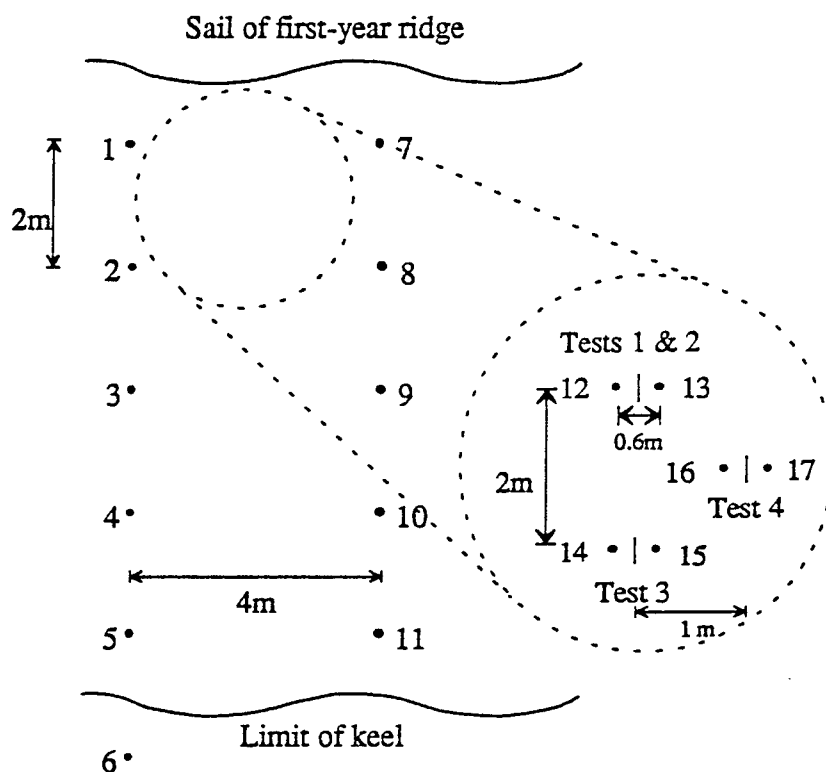


FIGURE 1. PLAN VIEW OF TEST SITE

The measured ice thicknesses in the refrozen lead and the ridge blocks were compared to values computed from ice camp temperatures using the formula for mean ice growth developed by Zubov (1944),

$$I^2 + 50I - 8R = 0 \quad (1)$$

in which I is the ice thickness in cm and R is the cumulative freezing degree days in °C-days using 0°C as a reference. As indicated in Figure 4, the lead was most likely formed during an ice motion event observed at the East Camp on March 26 and the ridge was probably formed during the storm and ice motion event observed at East Camp on March 30. The resulting ice thicknesses for the ridge blocks

are consistent with Zubov's formula. The formula under-predicted the lead ice thickness on April 14 by 17%.

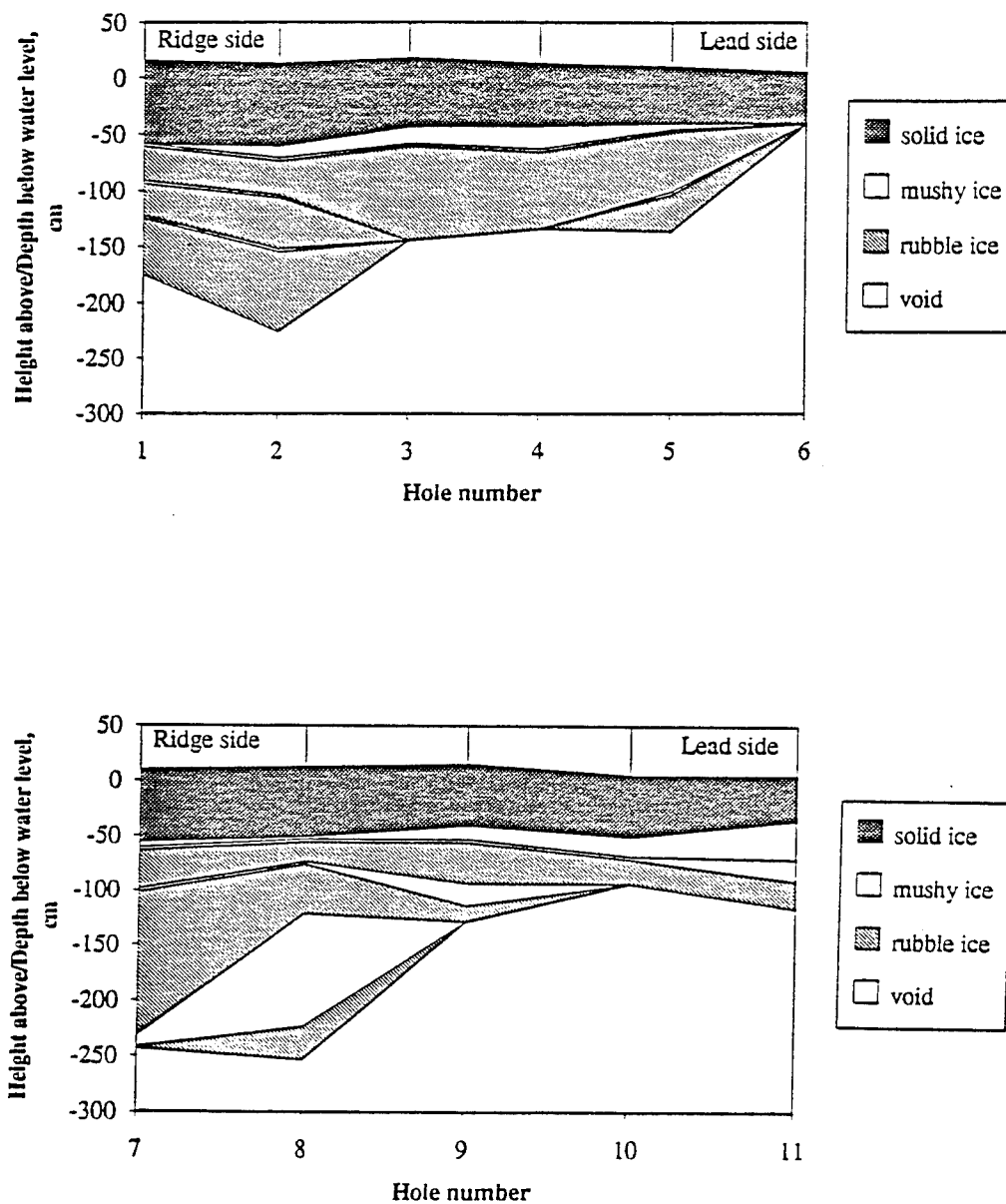


FIGURE 2. TWO KEEL CROSS-SECTIONS SHOWING VOIDS AS WHITE

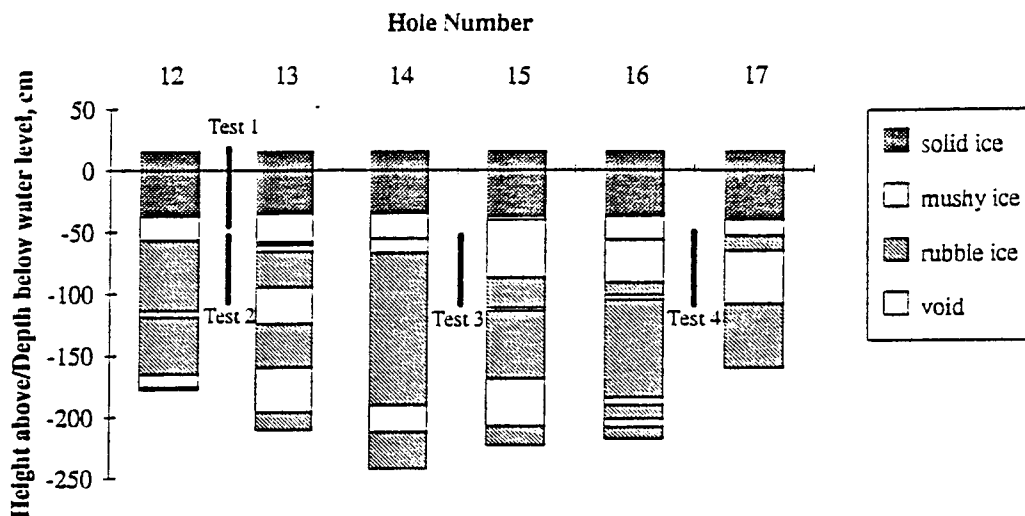


FIGURE 3. RELATIVE LOCATIONS OF THE AIR JACK TEST LOCATIONS AND THE SIX HOLES DRILLED ALONGSIDE THE AIR JACK SLOTS (VOIDS ARE SHOWN AS WHITE IN THE HOLES)

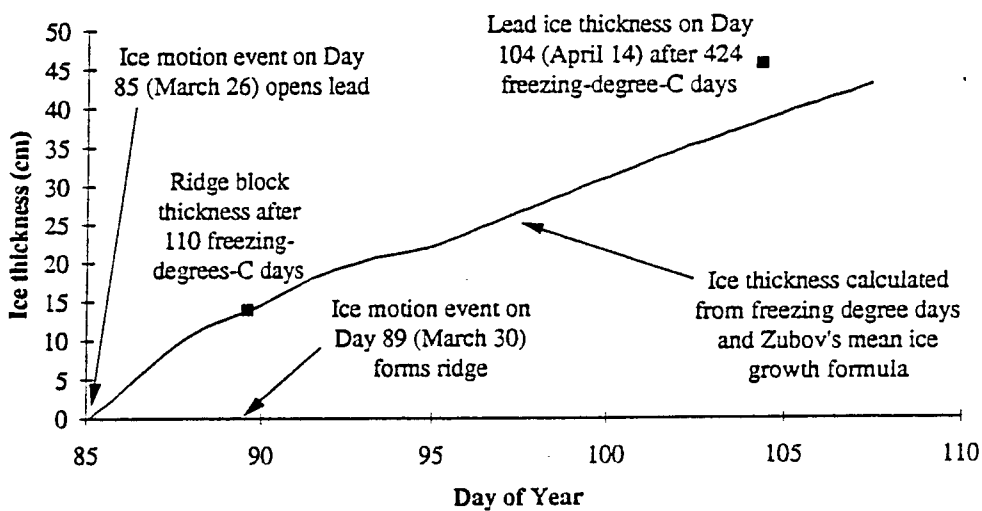


FIGURE 4. LEAD ICE THICKNESS IS CONSISTENT WITH OBSERVED ICE MOTION EVENTS

Temperature/salinity. Temperatures of blocks from the keel were measured with a thermistor; the results are provided in Table 1. The temperature measurements were obtained by drilling small holes into the ice blocks pulled from the first air jack slot, which extended down into the keel.

TABLE 1. TEMPERATURE AND SALINITY DATA

Location of reading	Temperature (°C)	Salinity (‰)
Sample from 15 cm below surface	-9.4	5.4
Sample from 40 cm below surface	-4.1	4.4
Sample from 75 cm below surface	-1.4	5.0

Salinity samples were taken from the same blocks; these results are also given in Table 1. A field study by Frederking and Wright (1982) indicate that 4-5 ‰ salinity is typical for submerged rubble.

Load tests

The load tests in the keel were performed with an air compressor inflating an air jack in a slot in the keel while recording the air pressure with a pressure transducer and a datalogger (see Figure 5). The air jack allowed a compact, light-weight system to deform the ice up to 30 cm (15 cm in each direction from the centerline) and measure the deformation. The test is analogous to the ice strength measurement test procedure described by Iyer and Masterson (1987) who froze thin-walled metal flat-jacks into multi-year ice to determine its strength.

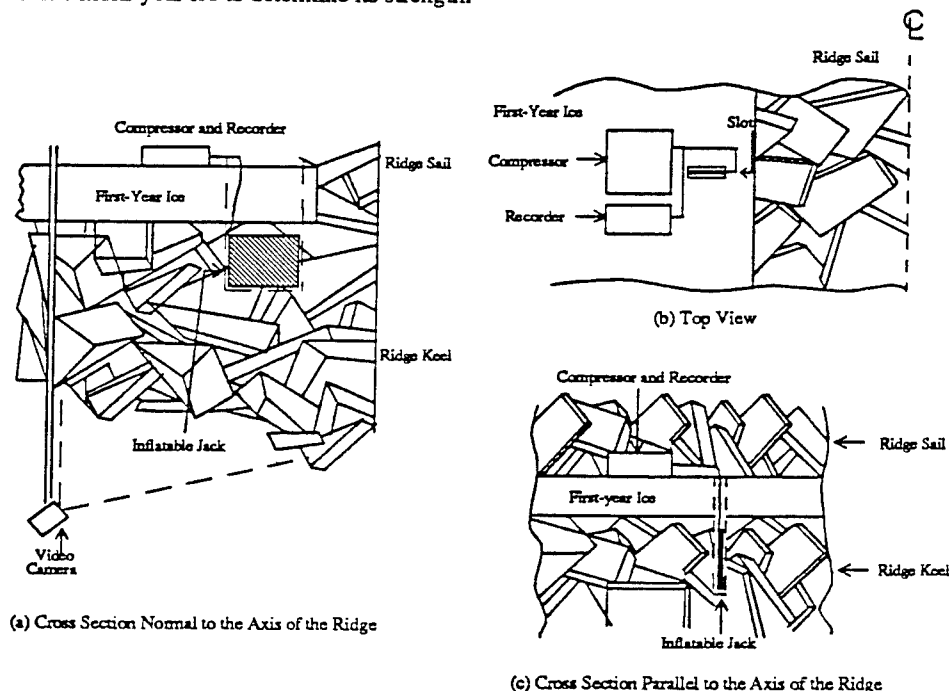


FIGURE 5. RIDGE STRENGTH EXPERIMENT

The jack displacement was derived from the compressor performance curve and the recorded pressure history by a series of laboratory calibration tests on the air compressor and the air jack. The slot for the air jack was cut with a modified wheel-mounted chain saw with a 1.5-m bar, as shown in Figure 6, made by the Ditcher Saw Company, Inc. Two cuts were made for each slot; the blocks of ice between were lifted from the slot for temperature and salinity measurements. From probing the slots, we know the slot cutting did not dislodge or free up the keel blocks.

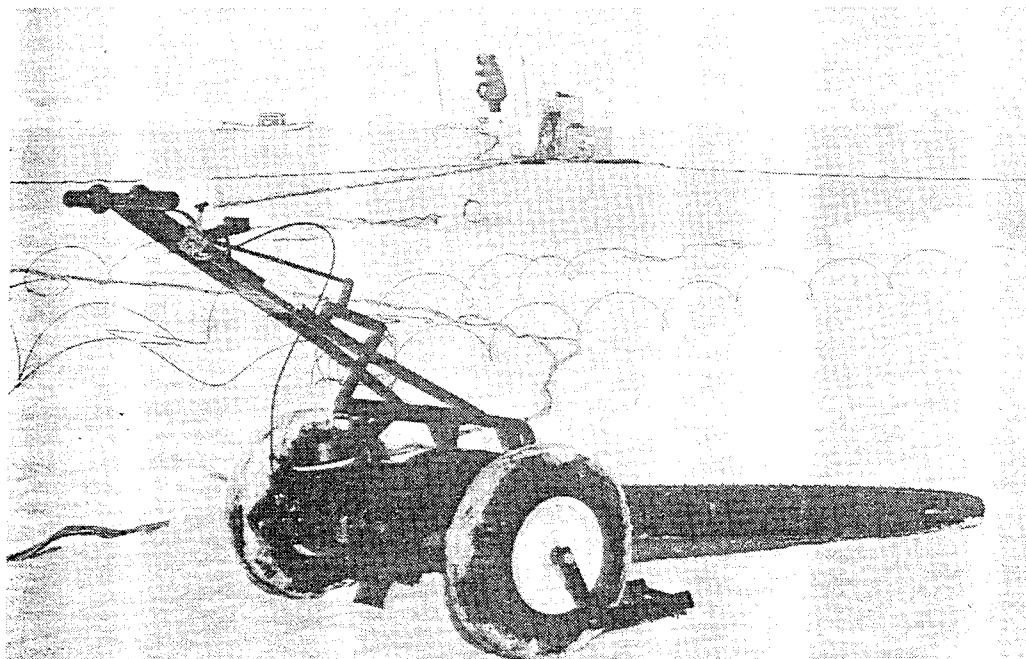


FIGURE 6. WHEEL-MOUNTED CHAIN SAW FOR CUTTING AIR JACK SLOTS

The Power Team air jacks used were 60x60x2 cm thick with a maximum rated pressure of 800 kPa and a displacement of 33 cm. We had no trouble dropping the air jack into these pre-cut slots in the manner shown in Figure 7. Once in the slot, the air jack was inflated by a small Black and Decker air compressor (for automobile tires) which operated off a 12V lead-acid gel-cell battery. The air pressure was measured with a factory-calibrated PSI-tronix pressure transducer and recorded with a Campbell Scientific CR-10 data logger and SM-192 storage module, which operated off a second 12V gel-cell battery.

We performed four inflation tests. As illustrated in Figure 3, the first test was in the consolidated layer, the second test was in the partially consolidated ice directly below it in the same slot, and the third and fourth tests were in the partially consolidated ice in separate slots. The top of the jack was 60 cm below the ice surface for the last three tests.



FIGURE 7. AIR JACK INSERTION

RESULTS

Pressure-displacement curves for the Northwest Research Associates tests from the spring of 1994 are shown in Figure 8. Both graphs in the figure show the same four tests, with different pressure scales. As seen in the figure, the strength of the partially consolidated ice in the ridge was highly variable on the scale of the air jack. Test 1 (in the top layer of consolidated ice) saw the highest pressures. It was stopped because of pressure/volume limitations of the air jack. Given the precision of the calculated displacement, we interpret Test 1 as having negligible displacement. The other three tests showed varying degrees of resistance to the jack and were stopped because of displacement conditions. All three show numerous displacement events at erratic time intervals. Test 3 had a large, abrupt displacement event with a corresponding rapid pressure drop (due to the expansion of the air in the jack) just before the compressor was stopped.

The fluctuations in air jack pressure (ram force) seen here are similar to those found in laboratory tests (e.g., Urroz and Ettema, 1987) despite the fact that the ratio of the ram size to ice block size is much smaller in these air jack tests. These fluctuations result from a combination of slip-stick block motion, breaking of cohesion bonds, and the ram stiffness. It is, therefore, necessary to average the results of numerous tests in the same ridge to increase the precision of the test results.

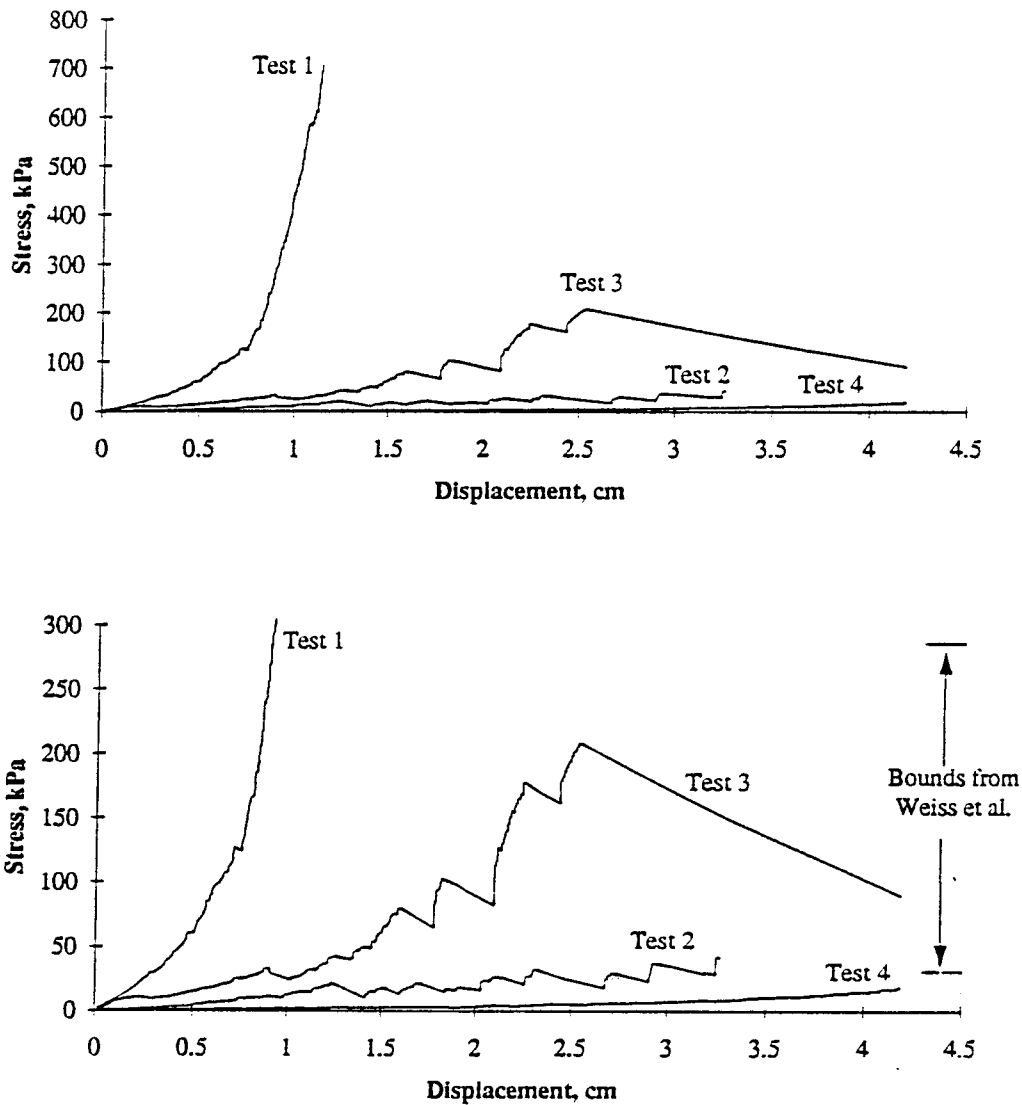


FIGURE 8. PRESSURE-DISPLACEMENT CURVES FOR RIDGE TESTS

RIDGE STRENGTH HINDCAST ANALYSIS

Laboratory test data from Weiss et al. (1981) were used with an analysis method from Coon et al. (1984) to hindcast the rigid-plastic limit load for Tests 2-4 in the partially consolidated portion of the keel. As shown in Table 2, the field test parameters matched quite well with the laboratory test parameters. The ridge ice blocks were slightly warmer with lower salinity, which is consistent with

being immersed in sea water for two weeks. Weiss reported their test results in terms of the Coulomb failure parameters: the effective angle of internal friction and the apparent cohesion.

TABLE 2. ANALYSIS PARAMETERS

Parameter	Laboratory data from Weiss et al. (1981)	SIMI ridge on April 14, 1995
Ice sheet thickness (cm)	15	14
Void ratio, η (porosity)	0.24 to 0.36	0.35
Ice block salinity (‰)	10 to 11	5
Ice block temperature (°C)	-2.5 to -5	-1.4
Displacement rate (mm/s)	3	0.4
Load area (m ²)	0.55	0.31
Consolidation state	Unconsolidated	Partially consolidated
Effective angle of internal friction, ϕ	26°	---
Apparent cohesion, C (kPa)	2.3	---

Figure 9a shows the plastic failure zone assumed for this analysis, and Figure 9b shows the corresponding Coulomb failure surface in Mohr space. The vertical dimensions in Figure 9a are based on the average values from the six drilled holes shown in Figure 3. The air jack or ram applies a uniform pressure, P_a , over a square area with the dimension, a , on a side just below the consolidated layer. The plastic failure zone extends down and away from the ram.

As an approximate solution to the problem shown in Figure 9, a closely related, plastic solution for Coulomb failure caused by a rectangular indenter will be used, after Coon et al. (1984). For this problem, the loaded area extends to the bottom of the keel as shown in Figure 10, in which the ice sheet is inverted to expose the bottom of the keel. A large volume of ice has been failed, and it is assumed that the load is on a half space. In Figure 10, there are three failing regions. ABCDEF moves in the direction of the load and up. The regions BHCF and ADGE move to the side and up. If it is assumed that the failure load of Figure 10 is the same as that of Figure 9a, then the indenter pressure, P_i , is smaller than the equivalent air jack pressure because of the load area difference

$$\text{Failure load} = P_i ah = P_a a^2 \quad (2)$$

The indenter failure pressure is given in Equation 17 of Coon et al. (1984) as

$$P_i = \sigma_c \left(1 + C_1(\phi) \frac{h}{a} \right) \quad (3)$$

where σ_c is the unconfined compressive strength of the Coulomb material and $C_1(\phi)$ is a correction coefficient derived in Coon et al. (1984) and presented graphically in Figure 11. From the geometry of the triangle in Figure 9b with β at one apex and 2κ at the other, the unconfined compressive strength is related to the apparent cohesion and effective angle of internal friction given in Table 2:

$$\sigma_c = \frac{2C \cos \phi}{1 - \sin \phi} \quad (4)$$

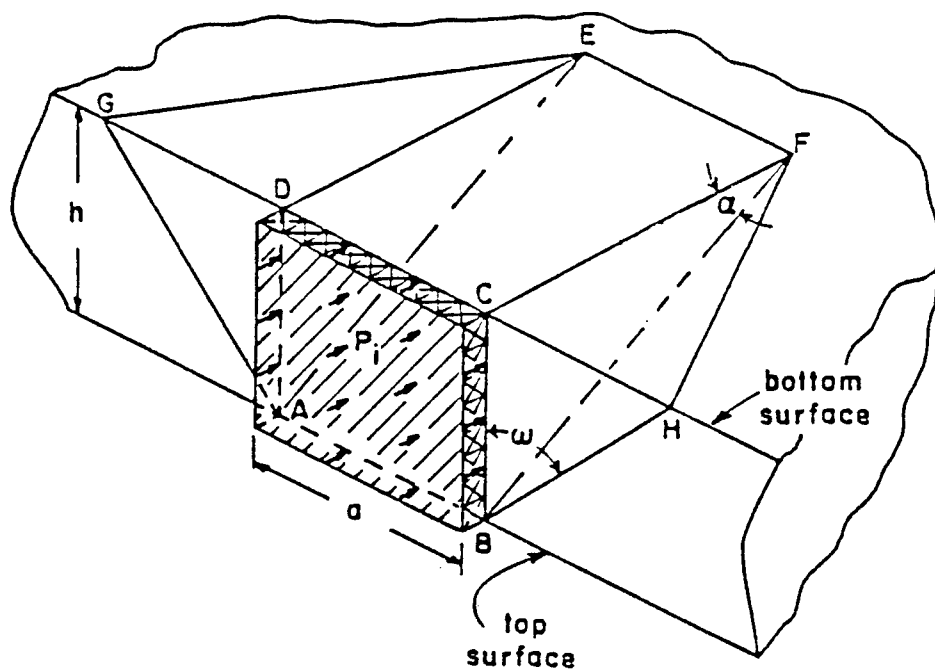


FIGURE 10. ASSUMED FAILURE MECHANISM FOR MOHR-COULOMB MATERIAL
(ADAPTED FROM FIGURE 11 IN COON, EVANS, AND GIBSON, 1984)

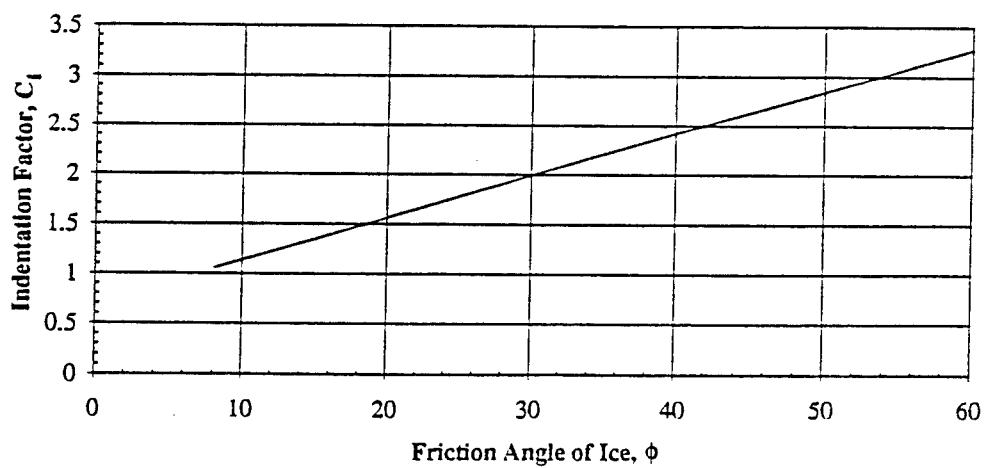


FIGURE 11. CORRECTION COEFFICIENT FROM COON ET AL. (1984)

Combining Equations 2, 3, and 4 yields

$$P_a = \frac{h}{a} \frac{2C \cos \phi}{1 - \sin \phi} \left(1 + C_1(\phi) \frac{h}{a} \right) \quad (5)$$

Table 3 includes a selection of solutions to Equation 5 using the dimensions from Figure 9a (167 cm for h , and 56 cm for a). Table 3 is examined row by row in the following. In the first row, the value of 26° for ϕ from Weiss et al. (1981) and the curve in Figure 11 are used to find a value of 1.8 for $C_1(\phi)$ and to predict a value of 140 kPa for the air jack pressure. The average jack pressure achieved in the three tests in the partially consolidated keel was 90 kPa. In the second and third rows in Table 3, the values for friction angle and cohesion were adjusted one at a time to match the air jack pressure from the tests. These all represent reasonable agreement considering the scatter in the three tests and the approximations made in the prediction.

In addition, Figure 12 compares our data to those of Weiss et al. (1981) for tests on similar size blocks. Figure 12 is adapted from Figure 3 in Weiss et al. (1981); the solid circles are the data from their slow tests. The solid line marked "slow" is their best fit through the slow data, and corresponds to the top row in Table 3. We have added four more lines, corresponding to the bottom four rows in Table 3. The last two rows in Table 3 are a lower bound and an upper bound for the Weiss "slow" data. The predicted air jack pressures from these bounds are 30 and 290 kPa; these two pressures are shown as horizontal lines in Figure 8. Tests 2 and 3 clearly fall within this range, and Test 4 may have as well if the test had been run to larger displacements.

TABLE 3. ANALYSIS RESULTS

Identification	Line number	Effective angle of internal friction, ϕ	Apparent cohesion, C (kPa)	Correction coefficient, $C_1(\phi)$	Air jack pressure from Eqn. 5 (kPa)
Weiss et al.	1	26	2.3	1.8	140
Adjust cohesion	2	26	1.5	1.8	90
Adjust angle	3	15	2.3	1.4	90
Lower bound	4	10	1	1.1	30
Upper bound	5	27	4.5	1.9	290

CONCLUSIONS AND DISCUSSION

The strength of the ridge keel in this experiment was tested at only one time; it is possible, however, to develop a clear picture of the keel strength from its formation to the time of the strength tests, as listed in Table 4. On March 30, the keel was formed with an overall depth of 220 cm comprised of a 14-cm ice sheet and a 206-cm unconsolidated keel. On April 14, the sheet was 53 cm thick near the test slots, leaving 167 cm of partially consolidated keel. For a strength comparison, it is assumed that the unconfined compressive strength of the ice sheet is 700 kPa, which is the horizontal unconfined compressive strength of unoriented columnar sea ice at a low strain rate taken from American Petroleum Institute (API) Bulletin 2N (1988). Although we stopped our test in this ice at 700 kPa, the limit load pressure of an air jack confined in this ice is related to the out-of-plane failure strength of the ice sheet, not the unconfined compressive strength. As indicated in Figure 9b, the compressive strength of the keel is calculated to be 7.4 kPa from Equation 4.

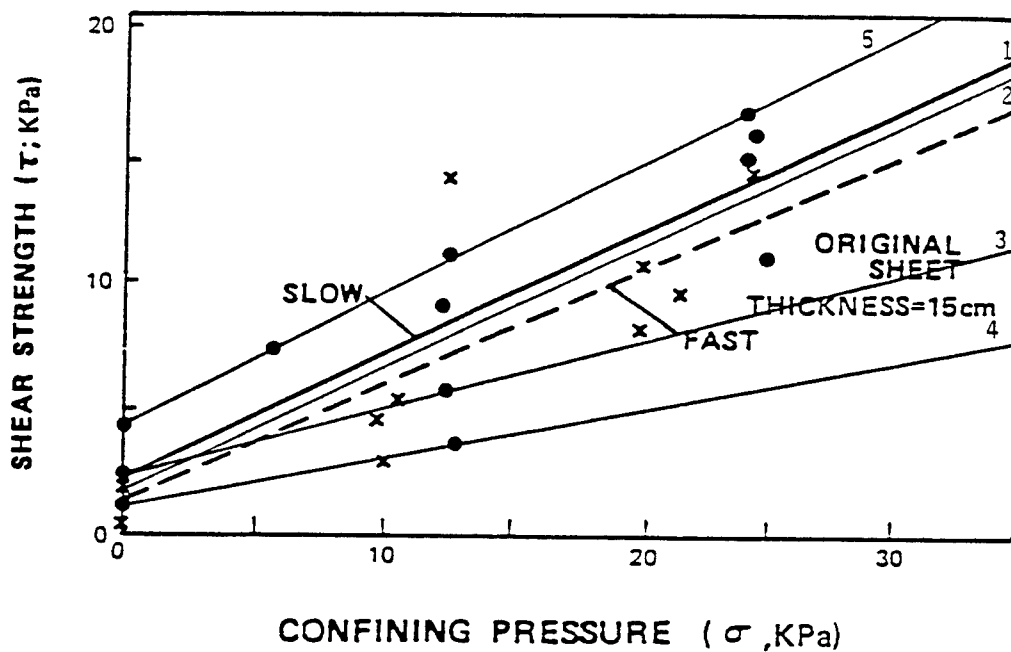


FIGURE 12. UNCONSOLIDATED ICE RUBBLE SHEAR STRENGTH (ADAPTED FROM WEISS ET AL., 1981)

Table 4. Ridge strength evolution

Parameter	March 30	April 14
Ice sheet thickness (m)	0.14	0.53
Keel thickness (m)	2.06	1.67
Ice sheet unconfined compressive strength (kPa)	700	700
Keel unconfined compressive strength (kPa)	7.4	7.4
Ice sheet strength resultant (kN/m)	98 (87%)	371 (97%)
Keel strength resultant (kN/m)	15 (13%)	12 (3%)
Total strength resultant (kN/m)	113 (100%)	383 (100%)

The strength resultant is the product of the strength and the depth. The values for compressive strength resultant in Table 4 are calculated using the unconfined strengths and depths in Table 4. It shows that the total unconfined strength of a unit width of the keel has increased by more than a factor of three from March 30 to April 14 and that the percentage contribution from the keel has decreased from 13% to only 3%. Therefore, it appears that the unconsolidated part of the keel contributed a

minor portion of ridge strength. However, it is important to remember there are very little field data on which to base this conclusion.

The variation of the stress-displacement curves for the partially consolidated keel in Tests 2-4 in Figure 8 imply that the jack size of 0.31 m^2 is not large enough to measure the average strength in a single test. This is not surprising given that the blocks had a thickness of 0.14 m with an average area of 0.20 m^2 with a standard deviation of 0.22 m^2 . It is desirable to have the jack size be much larger than the block size; this, however, requires very large equipment to make the slots and to install and inflate the large jack. It is reasonable to increase the size of a rectangular jack to about 1 m^2 and use it with a system that can be transported by helicopter. For field tests such as these, the transportability is very desirable. The load rate can be increased with a larger compressor. The larger jack also allows for a larger displacement, which helps determine when steady state motion is achieved in the tests. If many tests are run, then the average should be same as the result from a larger jack.

Our original plan was to test a ridge in the fall, winter, and spring to track strength with consolidation. That was not possible in this experiment but still seems to be a worthy objective.

ACKNOWLEDGMENTS

This work was done as part of the Office of Naval Research (ONR) Sea Ice Mechanics Initiative (SIMI). We thank Dr. Thomas Curtin of ONR for sponsoring this work as well as the overall SIMI Program. The authors also thank Andreas Heiberg, Jay Ardai, Dean Stewart, Steve Voorhees, and Suzanne O'Hara for their logistical support during the field program. The author's work was funded by ONR contract number N00014-92-C-0027.

REFERENCES

- Allyn, N., and B. R. Wasilewski, 1979, "Some Influence of Ice Rubble Field Formations Around Artificial Islands in Deep Water," in *Proceedings of 1979 Conference on Port and Ocean Engineering under Arctic Conditions*, Trondheim, Norway, Vol. 1, pp. 39-55.
- American Petroleum Institute, 1988, "Recommended Practice for Planning, Designing, and Constructing Fixed Offshore Structures in Ice Environments," API Recommended Practice 2N, First Edition, June 1, American Petroleum Institute Production Department, Dallas, TX.
- Coon, M. D., D. C. Echert, and G. S. Knoke, 1992, "Pack Ice Anisotropic Constitutive Model," in *IAHR 92, Proceedings of the 11th International Symposium on Ice*, Banff, Alberta, p. 1188.
- Coon, M. D., R. J. Evans, and D. H. Gibson, 1984, "Failure Criteria for Sea Ice and Loads Resulting from Crushing," in *Proceedings of IAHR Ice Symposium 1984 Hamburg*, Vol. III, pp. 1-16.
- Coon, M. D., G. S. Knoke, and D. C. Echert, 1994, "The Sea Ice Mechanics Initiative (SIMI)," in *Proceedings of the 26th Annual OTC Conference*, Houston, TX, May.
- Ettema, R., and J. A. Schaefer, 1986, "Experiments on Freeze-Bonding Between Floating Ice Blocks," *Journal of Glaciology*, Volume 32, No. 112, pp. 397-403.
- Ettema, R., and G. Urroz, 1989, "On the Internal Friction and Cohesion in Unconsolidated Ice Rubble," *Cold Region Science and Technology* 16, pp. 237-247.
- Frederking, R. M. W. and B. Wright, 1982, "Characteristics and Stability of an Ice Rubble Field, Issungnak, February-March 1980," NRC Technical Memorandum, Jan. 1982, No. 134, pp. 230-247.
- Iyer, S. H., and D. M. Masterson, 1987, "Field Strength of Multi-Year Ice Using Thin-Walled Flat Jacks," *Ninth International Conference on Port and Ocean Engineering Under Arctic Conditions*, Fairbanks, Alaska, pp. 57-73.
- Keinonen, A., and T. Nyman, 1978, "An Experimental Model Scale Study on the Compressible, Frictional and Cohesive Behavior of Broken Ice Mass," in *Proceedings of IAHR Symposium on Ice*, Luleå, Sweden, Vol. 2, pp. 335-353.
- Prodanovic, A., 1979, "Model Tests of Ice Rubble Strength," in *Proceedings of 1979 Conference on Port and Ocean Engineering under Arctic Conditions*, Trondheim, Norway, Vol. 1, pp. 89-105.

- Thorndike, A. S., D. A. Rothrock, G. A. Maykut, and R. Colony, 1975, "The Thickness Distribution of Sea Ice," *Journal of Geophysical Research*, Vol. 80, No. 33, pp. 4501-4513.
- Tucker, W. B., and J. W. Govoni, 1981, "Morphological Investigation of First-Year Sea Ice Pressure Ridge Sails," *Cold Regions Science and Technology*, No. 5, pp. 1-12.
- Urroz, G., and R. Ettema, 1987, "Simple Shear Box Experiments with Floating Ice Rubble," *Cold Region Science and Technology* 14, No. 2, pp. 185-199.
- Wang, A. T., and J. P. Poplin, 1995, "Challenges in Arctic Technology for Offshore Sakhalin Development," in *Proceedings of the Tenth International Symposium on Okhotsk Sea and Sea Ice*, Mombetsu, Hokkaido, Japan, February.
- Weiss, R. T., A. Prodanovic, and K. N. Wood, 1981, "Determination of Ice Rubble Shear Properties," in *Proceedings of IAHR International Symposium on Ice, Quebec*, Volume II, pp. 860-870.
- Wong, T. T., A. D. Gale, D. C. Sego, and N. R. Morgenstern, 1987, "Shear Box Tests on Broken Ice," in *Proceedings of the Ninth International Conference on Port and Ocean Engineering Under Arctic Conditions, POAC 87*, Fairbanks, Alaska, pp. 97-107.
- Zubov, N. N., 1944, *The Arctic Ice, Main Northern Sea Route*, Publishing House, 360 pp.

ACOUSTIC SIGNATURES OF FALLING ICE BLOCKS

ACOUSTIC SIGNATURES OF FALLING ICE BLOCKS

R. S. Pritchard
IceCasting, Inc.
Seattle, WA

Y. Xie and D. M. Farmer
Institute of Ocean
Sciences
Sidney, BC
CANADA

M. D. Coon, G. S. Knoke, and
D. C. Echert
Northwest Research Associates, Inc.
Bellevue, WA

ABSTRACT

During the April 1994 Sea Ice Mechanics Main Field Experiment, we conducted a set of *controlled-load* tests to mimic the small-scale processes that are active during the formation of rafts and ridges. Each test approximated the behavior of *in situ* sea ice, except that each process was isolated and the loading was artificially applied. In this paper we report results of the tests in which blocks of ice were dropped onto the ice sheet.

The acoustic signals emitted were separated into the forced acoustic wave generated by the first impact and the flexural oscillation of the floating ice sheet. For the forced impact, the total radiated acoustic energy is proportional to the kinetic energy at impact. When the ice sheet is bare (no snow cover), the ratio is about 11×10^{-6} . With a 1.3-1.5 cm snow cover, the ratio is about 2×10^{-6} . Variations in block size and ice sheet thickness are less important than the impact energy. The spectra were also determined for all tests. The snow cover reduced sound amplitude above 200 Hz by about 10 dB.

INTRODUCTION

As a ridge builds, there are numerous small-scale processes that occur: the ice sheet is bent, buckled, crushed, and cracked, blocks pile up and down, these same blocks tumble down and up along the sail and keel, blocks splash into the water, blocks are pushed over and under the ice, and the ice rafts. This last process is separated from over and under-ride because the ice blocks (and ice sheet) are pushed up and downhill, and the amount of wetness differs between over-ride and under-ride. It is difficult to quantify the physical processes that contribute to the noise generated during formation of a ridge because these processes occur simultaneously and in unknown amounts.

Of these processes, cracking has received extensive study (*e.g.* Stein, 1993). Our focus is on the other processes. Furthermore, when we listen to under ice noise, it is not cracking that dominates, but instead it is blocks falling against the ice sheet, and blocks sliding over and/or under the ice sheet, and rafting of ice sheets.

As one component of the April 1994 Sea Ice Mechanics Main Field Experiment (e.g., Coon et al., 1995, Xie and Farmer, and Pritchard, 1995), we conducted a set of *controlled-load* experiments. Each experiment approximated the behavior of *in situ* sea ice, except that one process was isolated and the loading was artificially applied. The *controlled-load* experiments included over-ride, under-ride, rafting, flopping, dropping, underwater bumping, and splashing. Each of these processes occurs during the formation of a ridge or raft. Each type of test is now described more completely: *over-ride* - towed a cold ice block over the surface of the intact ice sheet; *under-ride* - towed a warm ice block under the intact ice sheet; *raft* - towed a warm ice block (freshly excavated from refrozen lead ice) up and over a cantilevered beam section of the ice sheet; *drop* - dropped a block of ice (both flat and at a 45 degree angle) onto the intact ice sheet; *flop* - tipped a standing block of ice over onto the intact ice sheet; *splash* - tipped a standing block of ice over into the water; *bump* - allowed a submerged block of ice to float up and bump against the underside of the ice sheet; *cantilever* - lifted the free end of a floating cantilever beam until the beam failed in flexure; and *fracture* - split a floating ice sheet with air jacks.

Some of these processes affect the mechanical response of the ice, whereas all processes generate acoustic energy. The emission of waves from the impact is a valuable signal for probing the interaction process even though the emitted energy accounts for an extremely small amount of the input mechanical energy. The signal is useful from two points of view: it is readily measurable, and its signatures reflect the interaction process. The analyses of radiated signals allow possible reconstruction of such processes. Hydrophones, geophones, ice strain sensors, and ice tilt sensors were installed in arrays around the *controlled-load* tests.

The goal of this work is to understand the large-scale behavior of sea ice, and the noise emitted as it moves and deforms. The large-scale process that dominates ice behavior on this scale are rafting and ridging. Therefore we focus on these processes. Rafting is also a precursor to ridging. With better understanding of the small-scale mechanical processes that contribute to ridging and of the acoustic signals that are emitted by these processes, we hope to develop better models of ambient noise under the ice and inversely to use sound measurements as a gage to measure ice behavior. We envision a library of probability distribution signatures in phase space corresponding to the noise generation mechanisms. A general Arctic noise time series of an ice deformation event could then be partitioned into the library of events. The converse may also be possible, that is, to generate artificial or predictive time series of ambient noise that include the appropriate proportions of library signatures.

Here we present the acoustic signatures of these drop and flop tests. We estimate the acoustic emissions from individual processes, the spectral densities, and the ratio of total radiated acoustic energy to the mechanical input energy. The falling blocks studied here result from rearrangement of blocks in the ridge sail during the ridge building process. This redistribution was first modeled by *Parmerter and Coon* (1972) to match the angle of repose. The potential energy of the ridge was then incorporated explicitly by *Rothrock* (1975) into the Aidjex model. This and other energy measures were then used by *Pritchard* (1984, 1990) as a proxy variable for describing ambient noise generated by ridging. Finally, *Hopkins* (1994) estimated the energy balance during ridge building using a discrete element model of the forces acting on individual ice blocks in the ridge.

ACOUSTIC DATA ACQUISITION AND ANALYSIS

To investigate radiated energy from small-scale ice processes, an array of geophones and hydrophones were deployed at both East and West test sites from the Main camp. Figure 1 is a sketch of aerial view of the array deployed at East Camp. This array consisted of five tri-axial geophones (frozen into the ice surface) and the five omni-directional hydrophones (deployed at 5-m depth in the water). The maximum spacing of the array was approximately 30 meters. We are reporting on twelve tests at this site. A similar array was deployed on the West site. However, the West site array had a much greater maximum spacing of up to 200 meters; the hydrophones were deployed at 20-meter water depth. We are reporting on four tests at this site. Detailed descriptions of these arrays can be found in *Xie and Farmer* (1994a, 1995), *Coon et al.* (1995), and *Pritchard* (1995). For each test, acoustic and seismic emissions were digitally recorded on VHS tape.

To interpret the mechanical waves recorded on a sensor some distance away from the impact point, one must understand how the seismic and acoustic waves propagate in the Arctic environment. There have been extensive studies on various wave propagation mechanisms in the Arctic ocean (see *Stein*, 1993, *Xie and Farmer*, 1994b). There are two propagation channels for mechanical waves generated by the ice process: the floating ice sheet and acoustically up-refractive water column. The ice sheet guides various elastic waves in the ice. The water column provides signal channels for acoustic waves coupled into the water from the impacted local ice; it also allows the leakage of elastic waves from the ice sheet into the ocean. It has been shown that the characteristics of the guided elastic waves are mainly determined by the mechanical properties of the ice and its geometry, especially the

thickness. The elastic waves relevant to the present study are flexural waves, P-waves and SH-waves. The acoustic wave that is coupled directly from the ice impact has a signature that is affected both by the local ice properties and, most importantly, by the interaction process between the falling block and the ice sheet. It is the acoustic wave that provides more valuable information on the interaction process.

Both the SH-wave and flexural waves are trapped in the ice and upper water column due to horizontal polarization and subsonic phase velocities, respectively. However, P-waves leak into the water column in an efficient manner governed by Snell's law. Acoustic waves can propagate for a long distance (of order 10 km in a 500 meter deep water column) before being reflected from the bottom of the ice sheet. A layer of sea ice enriches the physics of underwater sound field in the Arctic ocean by projecting various elastic waves into the ocean. The co-existence of elastic (leaked from the ice) and acoustic (coupled directly from local failure processes in the ice) waves complicates the underwater sound field especially in the upper water column. From a signal detection point of view (in the water), one observes different signal structures arriving at different times, corresponding to the above described wave-process. With these theoretical descriptions and understandings of seismic and acoustic processes, we can examine the observed signals.

The total radiated acoustic power assuming a dipole distribution is

$$RA(t) = \int \frac{|p|^2}{\rho c} ds \quad (1)$$

where $p(r, \theta) = p_o \cos \theta / r$, ρc is acoustic impedance, θ is the radiation angle, p_o is source pressure observed at range r , and s is the spherical radiation area at range r . The total radiated acoustic energy is

$$TRAE = \int RA(t) dt \quad (2)$$

which can be rewritten using Parseval's equality as

$$TRAE = \int \frac{\cos^2 \theta}{r^2 \rho c} ds \cdot \left| 2 \int_0^{\infty} |\hat{p}_o(f)|^2 df \right| \quad (3)$$

where $\hat{p}_o(f)$ is the Fourier transform of $p_o(t)$.

RESULTS

On 8 April 1994 twelve drop tests were conducted at the East Camp and on 22 April 1994 four tests were conducted at West Camp. In each test a block of ice was either set on its edge and tipped so that it flopped onto its side or it was dropped onto the ice sheet. On 8 April the ice sheet was 0.25 m thick, it was covered by 1.3 cm of snow (although this was scraped off for some of the tests), temperature of the upper surface (under the snow) was -16.4 C, and the air temperature was -20 C. On 22 April the ice sheet was 0.51 m thick, covered by 1.5 cm of snow, and air temperature was -12.3 C.

A falling ice block dissipates its initial potential energy by interacting with the surrounding ice fields before reaching the minimum energy level. One of the common interacting modes is the impact of these free-fall ice blocks onto the surface of the underlying ice sheet. Xie and Farmer (1994b) found that a weight (an 11-kg lead ball) dropped onto a 2-meter thick first-year ice sheet created a dipolar acoustic source beneath the ice. Very small fractions of the total potential energy were radiated out from the impact as acoustic waves in the water column and flexural waves in the ice sheet. This implies that most potential energy of a falling weight is dissipated by deforming the local ice at the impact.

Figure 2 shows a time series of the acoustic signals for Test 8-1: an ice block flopping onto a snow-covered ice sheet. These signals were recorded by the array of five hydrophones deployed at the East site (see Figure 1). Since the impact occurred very close to H_1 (about 6 meters in range), the signal saturated this channel precluding estimation of acoustic source levels from this phone. Figure 3 is the acoustic signal due to a similar flopping test (Test 8-2) except that snow was cleared off from the ice surface before the test. These signals are discussed in the following three paragraphs.

The nearest hydrophone (H_1) was saturated for most tests. Channel H_2 was used for most analyses because it was farthest from the impact site and its signal had the best separation of acoustic and flexural waves. However, to see the flexural wave, we must look at H_1 or another hydrophone because the large, heavy data acquisition boxes were located along the path to H_2 , which reduced its flexural wave signal. We are interested primarily in

the dipole acoustic wave generated by the first impact because it propagates farther than the other signals.

The acoustic emissions recorded near the source by H_1 and shown in Figures 2 and 3 reveal that the impact generated two different vibrational responses in the ice sheet. These are motions forced by the impact and, subsequently, by the flexural response of the ice sheet. The impulse due to the forced motion couples directly into the water column and propagates at a speed of 1438 m/s in the water (we call this impulse signal the acoustic wave). Motions due to the flexural response of the ice spreads out as flexural waves from the impact point to the surround ice field (we call this flexural signal the seismic wave). Being an evanescent wave, the flexural motion is restricted in the ice sheet and upper water column. The wave travels in the ice at anomalously dispersive group speeds significantly lower than the sound speed in the water. Due to the shallow depths of the hydrophones, flexural wave signals can still be detected on these hydrophone channels. The speed difference between the acoustic wave (due to the initial impact) and flexural waves separates the arrivals of the two signals as they propagate. This effect is clearly illustrated by the wave signals recorded on channel H_1 in Figure 2: the acoustic signal arrives 58.7 ms ahead of the flexural wave, which yields a flexural group speed of 217 m/s. The dominant flexural wave frequency is estimated to be 20 Hz. This value is close to 250 m/s, a numerical result based on the dispersion curve obtained by Stein (1993). The signal amplitude is estimated from the first peak of the signal observed at hydrophone H_2 . This peak value is used to help isolate the flexural wave. The TRAE levels are presented in the Table I. The ratio of total radiated acoustic energy to the input energy is also presented.

The flop tests on snow-covered surface generated very little high-frequency acoustic radiation in the water. This implies that the snow layer makes the impact a soft landing on the ice sheet, absorbing high-frequency energy. Figure 2 shows the spectrum for a block flopping onto a snow-covered ice sheet and Figure 3 shows the spectrum for a block flopping over onto a bare ice sheet. The primary difference is the 10 dB reduction in sound above about 200 Hz.

The unique feature for falling tests is that the acoustic signatures radiated from these tests are more variable from test to test. Figure 4 shows the acoustic signals from a flat-dropping block. The signal consists of processes due to both forced motion by the impact and the flexural response of the ice sheet. However, the initial signal is no longer a single pulse but has a multi-pulse structure because the block shattered when it impacted the ice sheet. When falling at an angle, the ice block generated an even more complicated signal structure. An example is shown in Figure 5 where the signal due to forced motion is characterized by multiple pulses because the falling block bounced and shattered when it impacted the ice sheet. It is interesting to note that no significant flexural waves were excited by this impact.

For each test, block properties are presented in the Table I. These properties include: block size and shape (length L , width B , thickness H , and weight $W=Mg$, where M is mass), presence of snow, initial and final height of the center of gravity. The block sizes were representative of blocks observed in ridges (Tucker and Govani, 1981). The total energy input during each test is defined by the potential energy change $PE = PE_i - PE_f$, where potential energy at the beginning of the test was PE_i , potential energy at the end of each test was $PE_f = WH/2$. The kinetic energy at the moment of first impact was KE . For the flop tests, initial potential energy was

$$PE_i = \frac{W}{2}(L^2 + H^2)^{1/2}. \quad (4)$$

For the drop tests, initial potential energy was $PE_i = WZ$, where Z was the initial height of the center of gravity of the block. Kinetic energy at impact for the flop tests equals the change in potential energy. Kinetic energy at initial impact of blocks dropped flat onto the ice equals the difference between initial and final potential energy

$$KE = PE_i - PE_f \quad (5)$$

For blocks dropped from an initial angle of 45 degrees, the kinetic energy was equal to the difference between initial potential energy and potential energy at impact

$$KE = W(Z - \sqrt{2}(L + H)/4). \quad (6)$$

Table I. Parameters for Drop and Flop Tests.

Test No.	Test Type	L (m)	B (m)	H (m)	M (kg)	Snow	Initial CG Z(m)	Final CG (m)
8-1	Flop	0.50	0.50	0.25	60	Yes	0.28	0.13
8-2	Flop	0.50	0.50	0.25	60	No	0.28	0.13
8-3	Flop	1.00	0.50	0.25	120	No	0.52	0.13
8-4	Flop	0.53	0.51	0.10	24	No	0.27	0.05
8-5	Drop Flat	0.53	0.51	0.24	58	Yes	0.43	0.12
8-6	Drop Flat	0.53	0.51	0.24	58	No	0.73	0.12
8-7	Drop 45	0.48	0.51	0.24	56	No	0.61	0.12
8-8	Drop Flat	0.53	0.51	0.25	62	No	0.43	0.13
8-9	Drop Flat	0.43	0.36	0.06	9	No	1.25	0.03
8-10	Drop 45	0.51	0.46	0.10	24	No	1.22	0.05
8-11	Drop 45	0.53	0.51	0.08	24	No	0.61	0.04
8-12	Drop 45	0.99	0.53	0.10	49	Yes	0.91	0.05
22-4	Flop	0.51	0.48	0.07	15	Yes	0.26	0.03
22-5	Flop	0.49	0.50	0.15	38	Yes	0.26	0.08
22-6	Flop	0.51	0.48	0.07	15	No	0.26	0.03
22-7	Flop	0.49	0.50	0.15	38	No	0.26	0.08

Table II. Total Radiated Acoustic Energy (TRAE), Potential Energy (PE), and Impact Energy (KE) for Drop and Flop Tests.

Test No.	Test Type	PE (J)	KE (J)	TRAE (J)	TRAE/PE $\times 10^4$	TRAE/KE $\times 10^4$	Comments
8-1	Flop	89	89	0.000444	5.00	5.00	AE+Flexure
8-2	Flop	89	89	0.001034	11.64	11.64	AE+Flexure
8-3	Flop	459	459	0.004053	8.83	8.83	AE+Flexure
8-4	Flop	52	52	0.001171	22.50	22.50	AE+Flexure+1 bump
8-5	Drop Flat	172	172	0.000419	2.43	2.43	Double Impact
8-6	Drop Flat	344	344	0.002572	7.47	7.47	AE+Flexure+1 bump
8-7	Drop 45	268	194	0.001907	7.13	9.83	3 Impacts
8-8	Drop Flat	186	186	0.002341	12.60	12.60	AE+Flexure
8-9	Drop Flat	114	114	0.000961	8.44	8.44	AE+Flexure
8-10	Drop 45	275	237	0.000786	2.85	3.32	AE + Multi-bump
8-11	Drop 45	135	93	0.000277	2.06	2.98	AE + Multi-bump
8-12	Drop 45	419	256	0.000264	0.63	1.03	Multiple Impact
22-4	Flop	34	34	0.000010	0.29	0.29	AE
22-5	Flop	67	67	0.000055	0.82	0.82	AE
22-6	Flop	34	34	0.000516	15.15	15.15	AE - small bump
22-7	Flop	67	67	0.000985	14.70	14.70	AE - small bump

Parameters listed in the Table I were varied in an attempt to understand the physical behavior of falling blocks of ice. It was our desire to understand which variables affected the sound emitted and to quantify these effects.

All blocks dropped onto bare ice broke (tests 8-2 through 8-4, and 8-6 through 8-11). This was true whether flopped or dropped flat or at an angle. One result of such breaking was to generate multiple impacts from all pieces of the block, rather than clean single or double impacts when dropped flat or at an angle. Although the block in test 8-5 was initially level, it was dropped at an (unknown) angle, which caused a double impact. Test 8-7 was dropped at an angle and produced two distinct impacts; first when the edge hit the ice sheet, and second when it flopped over flat.

We assume that a relationship exists between the total energy radiated by the acoustic waves and the energy input by dropping the block, and we test this hypothesis. The energy available from dropping the block is easily estimated by calculating the change in potential energy before dropping the block and the instant it impacts the ice sheet. This calculation is somewhat different for the various geometries.

The *TRAE* is compared directly with the impact kinetic energy (*KE*) in Figure 6. Open symbols indicate ice blocks falling onto snow-covered ice; black symbols onto bare ice. Different symbol shapes have been used to identify the different kinds of tests (flat drop - square, drop at 45 degrees - diamond, and flop - triangle). For all drops on a bare ice sheet, the average ratio of *TRAE* to potential energy was 11×10^{-6} . Two data points (tests 8-10 and 8-11) had lower ratios. Both of these ice blocks shattered, which likely cause the lower *TRAE* values. When snow is present, the average ratio of *TRAE* to potential energy is reduced to 2×10^{-6} . These results appear to be consistent over the full range of impact energy.

The data were also examined for correlations with block area, mass, test type, and angle of the drop. None were as strong as variations with snow cover. We recognize of course that this is a small test set, and definitive correlations are difficult. For the lead ball used by *Xie and Farmer (1994a)*, the average ratio of *TRAE* to potential energy was about 20×10^{-6} , so that ice blocks are less than half as efficient at generating acoustic energy as the idealized spherical lead ball. We noted earlier that these block sizes are representative of ice blocks found in ridges. We note here that the range of distances from which they were dropped (0.15-1.22 m) is also representative of distances that blocks fall during ridging. We have also compared the total change in potential energy, but the ratio between *TRAE* and *PE* is not as consistent as is the ratio of *TRAE* to *KE*.

CONCLUSION

Sixteen tests were conducted in which ice blocks were either dropped or flopped onto the ice sheet. The acoustic signals emitted were separated into the forced acoustic wave generated by the first impact and the seismic wave generated as a flexural oscillation of the floating ice sheet. We focused analysis on the acoustic wave that has approximately a dipole pattern. It propagates to longer ranges than does the flexural wave.

When the ice blocks were dropped at an angle, several distinct impacts observed. When the blocks were dropped onto bare ice they broke, which also generated multiple impacts.

The total radiated acoustic energy was found to be proportional to the kinetic energy at impact. When the ice sheet was bare (no snow cover), the ratio was about 11×10^{-6} . With a 1.3-1.5 cm snow cover, the ratio was about 2×10^{-6} . Variations in block size and shape appeared to be less important than the impact energy. There was no apparent dependence on ice sheet thickness (over the range 0.25-0.51 m) for the first impact acoustic signal studies here. We would expect such a dependence to exist for the flexural wave. The spectra were also determined for all tests. The snow cover reduced sound amplitude above 200 Hz by about 10 dB.

These results suggest that a model could be developed to describe the acoustic emission from the blocks falling during formation of a ridge. The model would require that we estimate the kinetic energy available for blocks falling onto the ice sheet and the probability distribution of events, but these variables can be estimated from modern ice dynamics models.

ACKNOWLEDGMENTS

This study was funded by the Office of Naval Research (ONR) under contracts N00014-C-92-0052 to IceCasting, Inc., N00014-J-92-1256 to the Institute of Ocean Sciences, and N00014-C-92-0027 to NorthWest Research Associates, Inc. All authors greatly appreciate the encouragement and support given by Dr. T. B. Curtin, ONR High Latitude Team Leader. We also thank A. Heiberg, J. Ardai, D. Stewart, and S. Vorhees for their support in the field.

REFERENCES

- Coon, M. D., Knoke, G. S., and Echert, D. C., *Sea Ice Mechanics Research*, presented at Sea Ice Mechanics and Arctic Modeling Workshop, Anchorage, April 25-28, 1995.
- Farmer, D. M., and Xie, Y., *Acoustic and Seismic Studies of Ice Mechanics*, presented at Sea Ice Mechanics and Arctic Modeling Workshop, Anchorage, April 25-28, 1995.
- Hopkins, M. A., "On the Ridging of Intact Lead Ice," *J. Geophys. Res.*, vol. 99, pp. 16351-16360, 1994.
- Parmerter, R. R., and Coon, M. D., "Model of Pressure Ridge Formation in Sea Ice," *J. Geophys. Res.*, vol. 77, pp. 6565-6575, 1972.
- Pritchard, R. S., "Sea Ice Noise-Generating Processes," *J. Acoust. Soc. Am.*, vol. 88, no. 6, pp. 2830-2842, 1990.
- Pritchard, R. S., "Arctic Ocean Background Noise Caused by ridging of Sea Ice," *J. Acoust. Soc. Am.*, vol. 75, pp. 419-427, 1984.
- Pritchard, R. S., "Sea Ice Failure Mechanisms," presented at Sea Ice Mechanics and Arctic Modeling Workshop, Anchorage, April 25-28, 1995.
- Rothrock, D. A., "The Energetics of the Plastic Deformation of Pack Ice by ridging," *J. Geophys. Res.*, vol. 80, no. 33, pp. 4514-4519, 1975.
- Stein, P. J., "Prediction and Measurements of the Directivity of a Monopole Source in a Floating Ice Plate," in *Natural Physical Sources of Underwater Sound (2)*, ed. B. Kerman, Kluwer Academic Press, Norwell, MA, 1993.
- Tucker, W. B., III, and Govani, J. W., "Morphological Investigation of First-Year Sea Ice Pressure Ridge Sails," *Cold Regions Science and Technology*, No. 5, pp. 1-12, 1981.
- Xie, Y and D. Farmer, *Acoustic and seismic perspective of ice events observed in SIMI '94 Experiment A* report to the Office of Naval Research, published at Institute of Ocean Sciences, Sidney, BC, Canada, December, 1994a.
- Xie, Y. and D. M. Farmer, "Seismic-acoustic Sensing of sea ice wave-mechanical properties," *J. Geophys. Res.*, Vol 99, No. C4, pp 7771-7786, 1994b.

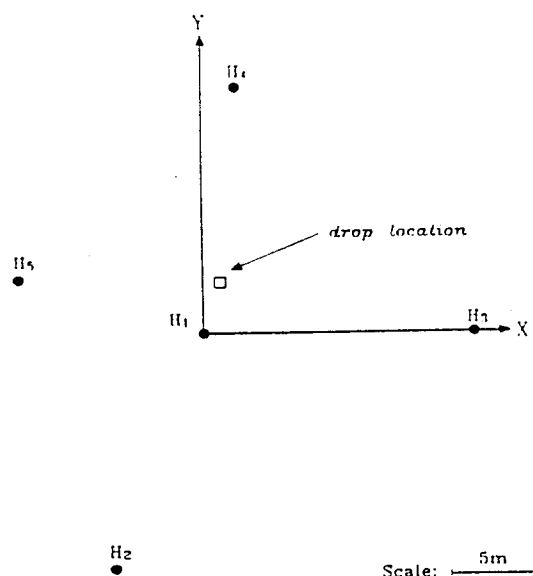


Figure 1. Hydrophone Array at SIMI East Camp.

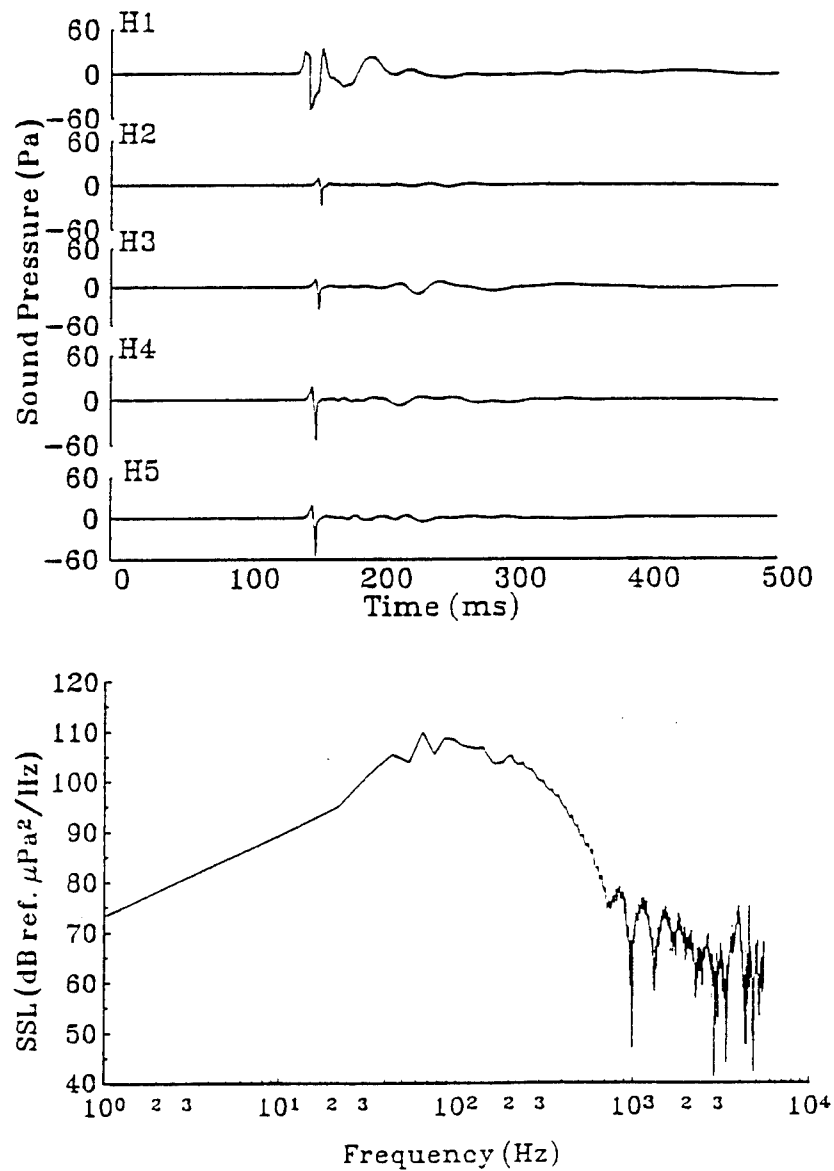


Figure 2. Sound Emitted by Ice Block Flopping Onto Snow-covered Ice Sheet (Test 8-1). Top: Pressure History at Five Hydrophones. Bottom: Sound Spectrum Level (SSL) at Hydrophone H₁.

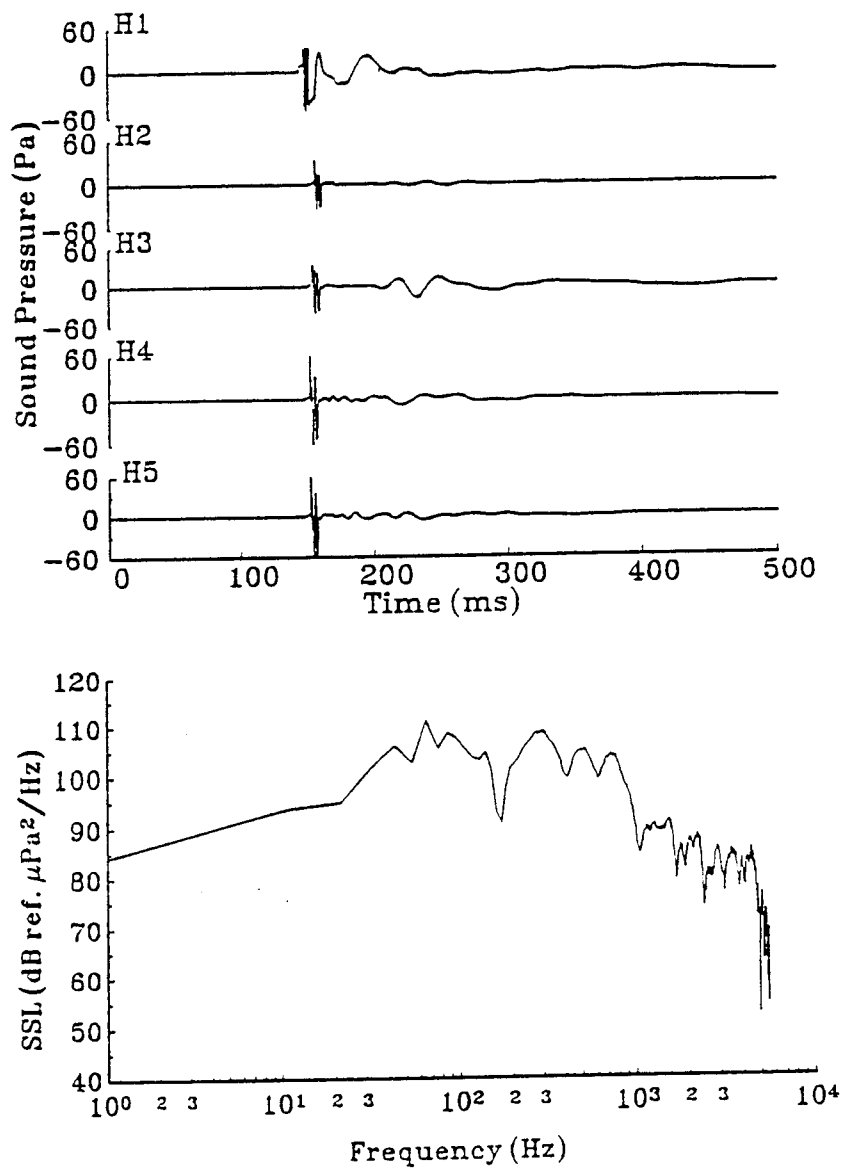


Figure 3. Sound Emitted by Ice Block Flopping Onto Bare Ice Sheet (Test 8-2). Top: Pressure History at Five Hydrophones. Bottom: Sound Spectrum Level (SSL) at Hydrophone H₂.

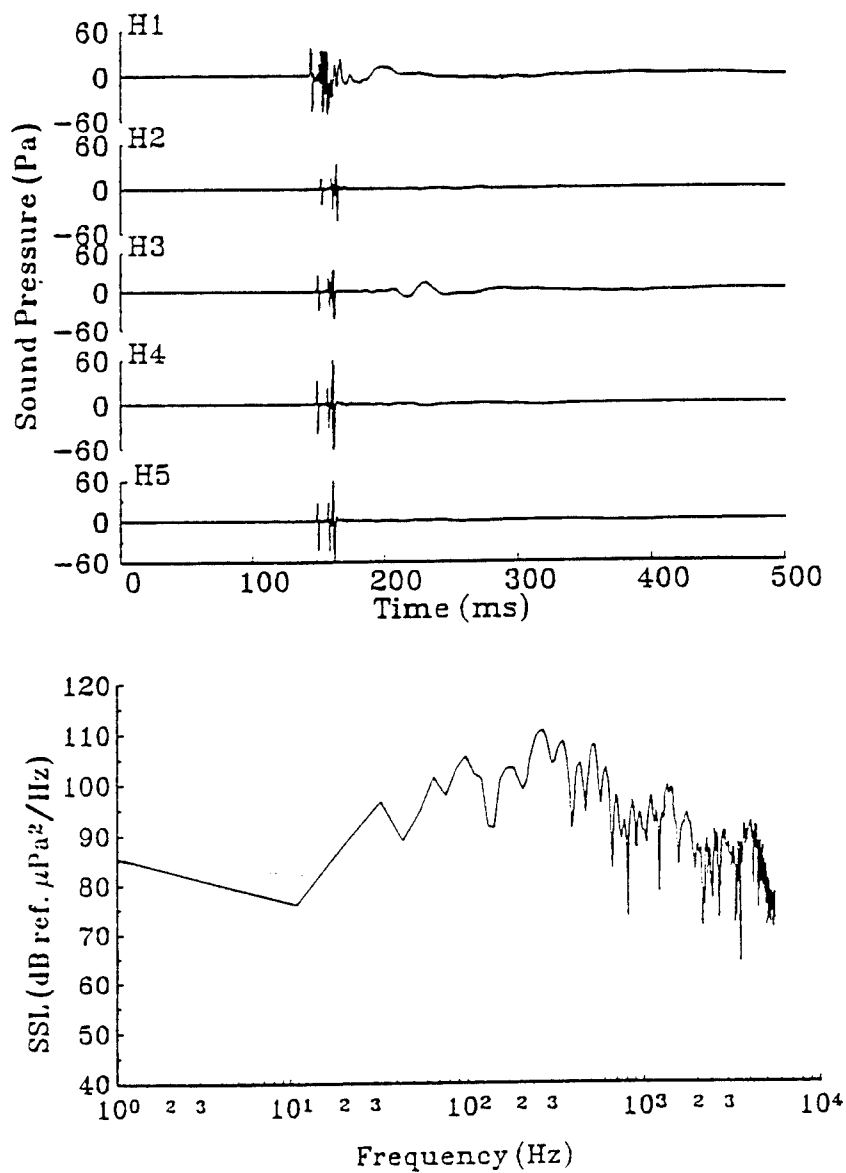


Figure 4. Sound Emitted by Ice Block Dropping Flat onto Bare Ice Sheet (Test 8-9). Multiple Impacts Result from Shattering of the Ice Block. Top: Pressure History at Five Hydrophones. Bottom: Sound Spectrum Level (SSL) at Hydrophone H₁.

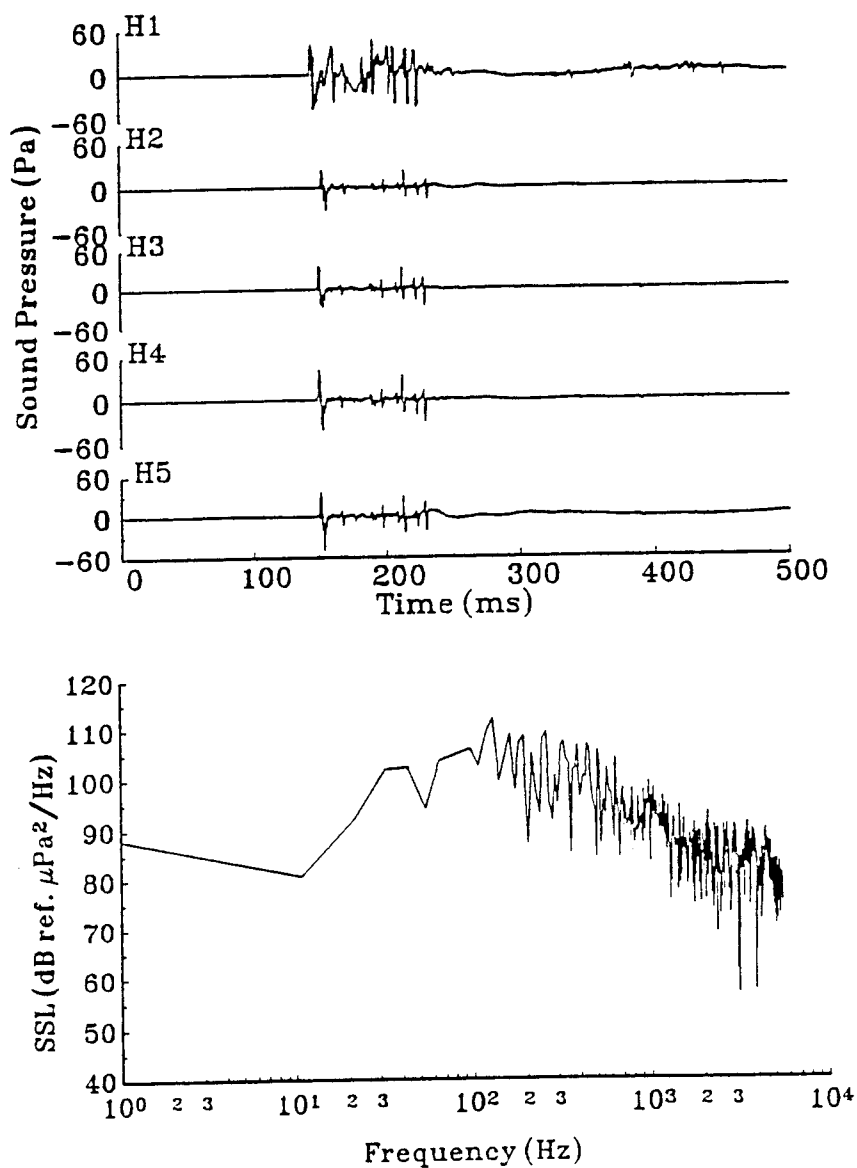


Figure 5. Sound Emitted by Ice Block Dropping at 45 Degree Angle onto Bare Ice Sheet (Test 8-10). Multiple Impacts Result from Initial Angle of Drop and Shattering of the Ice Block. Top: Pressure History at Five Hydrophones. Bottom: Sound Spectrum Level (SSL) at Hydrophone H₂.

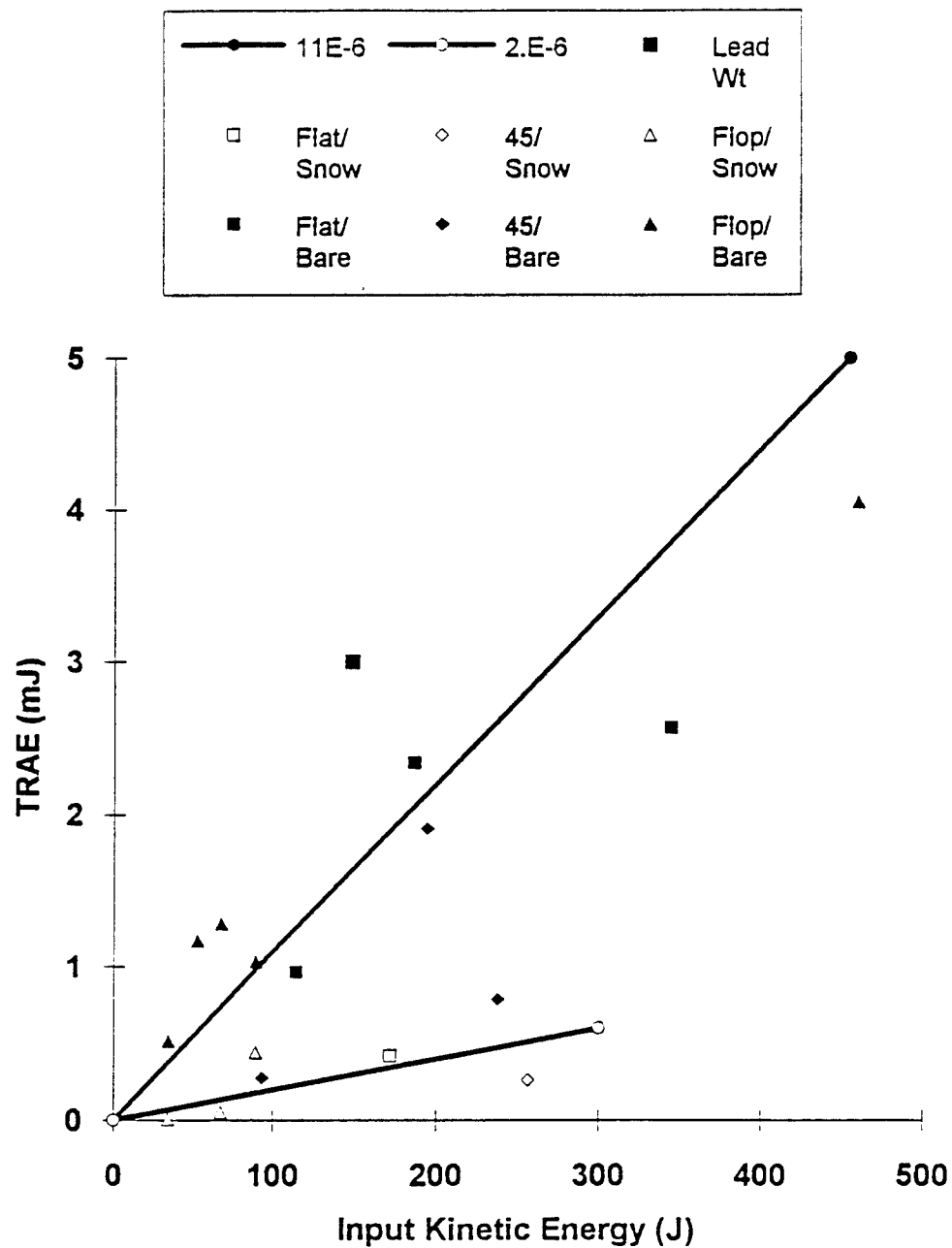


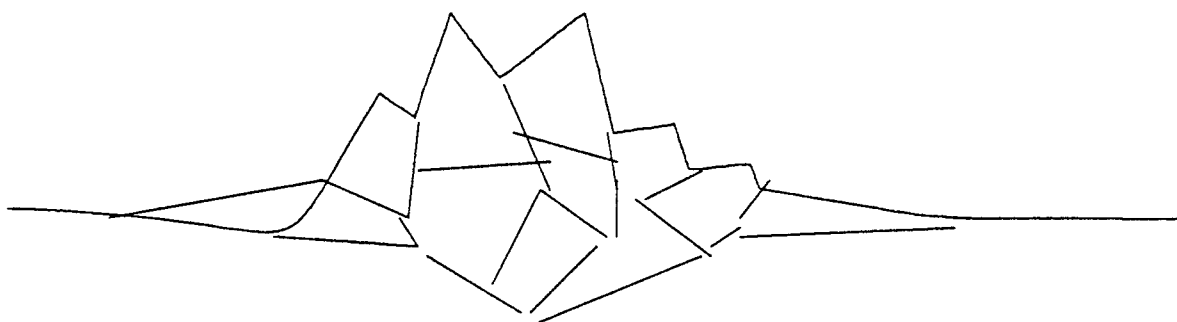
Figure 6. Relationship Between Total Radiated Acoustic Energy (*TRAE*) and Input Kinetic Energy (*KE*). Ice Blocks Dropped onto Bare Ice had a Ratio (*TRAE/KE*) of 11×10^{-6} . Ice Blocks Dropped onto Snow-covered Ice had a Ratio of 2×10^{-6} . A Lead Ball Weight had a Ratio of About 20×10^{-6} .

*PROCEEDINGS OF THE
SEA ICE MECHANICS
AND ARCTIC MODELING WORKSHOP*

**Proceedings of the
Sea Ice Mechanics and Arctic Modeling Workshop**

April 25-28, 1995, Hilton Hotel, Anchorage, Alaska

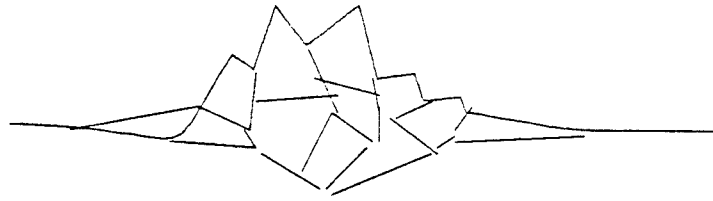
Volume 1



Sponsored by

U.S. Minerals Management Service,
U.S. Navy Office of Naval Research,
Canadian National Energy Board,
and Participating Members of the Oil Industry:
Amoco, Arco, Chevron, and Mobil

Organized by Northwest Research Associates, Inc.
Bellevue, WA



Sea Ice Mechanics and Arctic Modeling Workshop Volume 1

Table of Contents

1. Introduction
2. Acoustics
 - Farmer, D., and Y. Xie, "Acoustic and Seismic Studies of Ice Mechanics"
 - Mikhalevsky, P., A. B. Baggeroer, H. Schmidt, K. von der Heydt, E. K. Sheer, and A. Gavrilov, "Transarctic Acoustic Propagation"
 - Pritchard, R. S., "Sea Ice Failure Mechanisms"
 - Rajan, S. D., "Sea Ice Mechanics Research: Tomographic Imaging of Wave Speeds and Acoustic Emission Event Localization"
 - Schmidt, H., A. B. Baggeroer, I. Dyer, K. von der Heydt, and E. K. Scheer, "Seismo-Acoustic Remote Sensing of Ice-Mechanical Processes in the Arctic"
 - Stein, P. J., D. W. Andersen, A. Bahlavouni, S. E. Euerle, G. M. Santos, and R. K. Menoche, "SIMI Winter-Over Geophone/Hydrophone System"
3. Fracture Mechanics
 - Bažant, Z. P., Y.-N. Li, M. Jirásek, Z. Li, and J.-J. Kim, "Effect of Size on Distributed Damage and Fracture of Sea Ice"
 - Dempsey, J., and R. Adamson, "Scale Effects on the Fracture and Constitutive Behavior of Sea Ice"
4. Ice Properties
 - Cole, D. M., "Field and Laboratory Experiments and Modeling of the Constitutive Behavior of Sea Ice"
 - Gupta, V., R. C. Picu, J. Bergström, and H. J. Frost, "Crack Nucleation Mechanisms in Columnar Ice -- Recent Developments"
 - Schulson, E. M., "Compressive Failure of Columnar Saline Ice under Multiaxial Loading"
 - Shapiro, L. H., W. F. Weeks, and W. D. Harrison, "Studies of the Influence of Fabric and Structure on the Flexural Strength of Sea Ice and, of the Consolidation of First-Year Pressure Ridges"

5. Ice Stress, Ice Strain, and Ice Conditions
 - Coon, M. D., D. C. Echert, and G. S. Knoke, "Sea Ice Mechanics Research"
 - O'Hara, S. and J. Ardai, Jr., "SIMI GPS Position and CTD Cast Data"
 - Overland, J., S. Salo, S. Li, and L. McNutt, "Regional and Floe-Floe Deformation"
 - Richter-Menge, J. A., B. C. Elder, W. B. Tucker III, and D. K. Perovich "Pack Ice Stresses and their Relationship to Regional Deformation"
6. Modeling
 - Connor, J. J., S. Shyam-Sunder, A. Elvin, D. Choi, and J. Kim, "Physically Based Constitutive Modeling of Ice"
 - Hopkins, M. A., "Numerical Simulation of Arctic Pressure Ridging"
 - Lewis, J. K., and P. J. Stein, "Sea Ice Mechanics Related to Thermally-Induced Stresses and Fracturing of Pack Ice"
 - Petrenko, V., and O. Gluschenkov, "Measurements of Crack Velocity in Sea Ice Using Electromagnetic Techniques"
 - Rodin, G., R. Shapery, K. Abdel-Tawab, and L. Wang, "Constitutive Equations and Fracture Models for Sea Ice"
 - Wu, M. S., J. Niu, Y. Zhang, and H. Zhou, "Physically-Based Constitutive Modeling of Ice: Damage and Failure"

Appendix A -- Air-Ice-Ocean Interaction: Lead Dynamics, Ice Mechanics, Ice Acoustics
(Sea Ice Mechanics Workshop at Airlie, VA, 1990)

Appendix B -- Sea Ice Mechanics Initiative (SIMI) Summary Plan, FY94-95 (Workshop
at Sidney, BC, 1993)

Front cover: A first-year ridge in the Beaufort Sea near the SIMI East Camp (photo by
M. Coon)

Rear cover: Site of ice fracture tests near the SIMI East Camp (photo by S. Echert)

1. INTRODUCTION

The Sea Ice Mechanics and Arctic Modeling Workshop to be held in Anchorage, Alaska, April 25-28, 1995, will focus on current state of the practice and future research needs relative to offshore oil and gas facilities and will also review the results of the U.S. Navy's Office of Naval Research (ONR) Sea Ice Mechanics Initiative (SIMI). SIMI is a continuing ONR program running from October 1992 through September 1996, with sea ice mechanics and Arctic acoustics field programs, laboratory studies, and modeling work. The SIMI goals are to understand sea ice constitutive laws and fracture mechanics over the full range of geophysical scales, to determine the scaled responses to applied external forces, and to develop physically based constitutive and fracture models. The goals were established at a SIMI planning meeting held at Airlie, Virginia, in November 1990. The report from that meeting is included as Appendix A. The main field experiments were defined at a second SIMI planning meeting held at Sidney, British Columbia, in August 1993 and are described in the Summary Plan included as Appendix B. The main field experiments were conducted in the Beaufort Sea during 1993 and 1994.

Volume 1 has four major parts:

1. Four ice maps: the fall and spring SIMI camps at 2-km and 10-km scales (included in this section).
2. Summaries of poster presentations by the SIMI Principal Investigators of their findings to date, their model developments, their data sets, and their upcoming publications. These are divided into five sections focusing on broad topics. Each section begins with a list of the papers in the section and a list referring the reader to papers in other sections containing information on the same subject.
3. Proceedings of the first SIMI planning meeting (as Appendix A).
4. The SIMI Summary Plan (as Appendix B).

After the workshop, NWRA will publish the invited lectures and working-group summary presentations and recommendations in Volume 2.

Volume 1 is organized as follows. Section 2 includes the summary papers on Arctic acoustic experiments. Sea ice fracture mechanics papers are in Section 3. Laboratory and field studies of sea ice properties are in Section 4. Section 5 presents investigations of pack ice stress, ice strain, and other observations, such as CTD casts. Section 6 includes the various sea ice modeling studies. There is a cross-reference list of papers at the beginning of each section.